Elastic and inelastic scattering of polarized protons from ^{206}Pb near isobaric analog resonances

N. L. Back* and J. G. Cramer†
Nuclear Physics Laboratory, University of Washington, Seattle, Washington 98195
(Received 16 March 1983)

Excitation functions have been measured for the elastic and inelastic scattering of polarized protons from ^{206}Pb at $\theta_{lab}=120°$, 135°, 150°, and 165° in the energy range $E_p=14.25-18.00$ MeV. Excellent fits to the elastic scattering data were obtained using a parametrized background and the isobaric analog resonances of 35 states in ^{207}Pb (the "parent states") with $E_x=2.3-5.7$ MeV; spin-parity assignments and resonance parameters were determined for all of these isobaric analog resonances. The data for inelastic scattering to the first excited state (2^+, 0.803 MeV) were described using a distorted-wave Born approximation background and the same isobaric analog resonances; good fits to the data were obtained by varying only the inelastic partial width amplitudes. A set of spectroscopic amplitudes was then found, for both the single-particle and the particle-core components of the parent states, by comparing the best-fit resonance parameters with those given by model calculations. The internal consistency of this set was verified by using sum rules. The spectroscopic amplitudes are compared with those given by simple weak-coupling model predictions; there is considerable disagreement, probably because too few configurations were used in the theoretical calculations.

[NUCLEAR REACTIONS ^{206}Pb($\vec{p}$,p), ($\vec{p}$,p'), $E=14.25-18.00$ MeV; measured $\sigma(E;\theta)$, $A_y(E;\theta)$; deduced isobaric analog resonance parameters. ^{207}Pb deduced J,π, single-particle and particle-core spectroscopic amplitudes for 35 levels.]

I. INTRODUCTION

The isobaric analog resonance (IAR) showed early promise of becoming a valuable spectroscopic tool for studying the structure of medium-weight and heavy nuclei, particularly in the vicinity of closed-shell nuclei such as ^{208}Pb.[1-8] With the advent in recent years of high-intensity sources of polarized protons, this promise has now been fully realized. By measuring both the cross section and the analyzing power in the vicinity of an IAR, an experimenter can obtain twice as much information as he could by measuring the cross section alone. Moreover, the additional information provided by the analyzing-power data is particularly valuable in determining the spin of the IAR,[9] as well as in studying interference effects, both between the IAR and the nonresonant background and between overlapping IAR's.

Previous polarized-beam experiments,[10-13] using ^{208}Pb, ^{207}Pb, and some $N=82$ nuclei as targets, have been very successful in exploiting these advantages, not only for elastic scattering but also for inelastic scattering to some low-lying collective states. For these states, the interference between the direct background and the IAR resulted in a nonzero analyzing power; this made it possible to obtain reliable spectroscopic information from the inelastic scattering data. In previous unpolarized-beam experiments, on the other hand, this same interference had been a severe complicating factor which had made it difficult to analyze the data and rendered questionable the resulting spectroscopic information.

In this paper, we describe a similar experimental study, in which ^{206}Pb was used as the target. We were able to obtain information on the structure of a number of states in ^{207}Pb (the "parent states") by observing the proton decays of their IAR's to the ground state and to the first excited state (2^+, 0.803 MeV) of ^{206}Pb. This information is presented here using the language of the weak-coupling model,[14] with each of the parent states written as a linear combination of simple configurations, each of which consists of a single neutron coupled to a particular state of ^{206}Pb,

$$|\Pi_j\rangle=\theta_{0,lj}\,|0^+\otimes lj\rangle + \sum_{j'}\theta_{2^+,l'j'}\,|(2^+\otimes l'j')_j\rangle+\cdots . \quad (1)$$

In this expression, the parent state $|\Pi_j\rangle$ (with spin j) is represented as the sum of (1) a single-particle configuration, (2) a number of configurations in which a single neutron is coupled to the first excited state of ^{206}Pb, and (3) additional particle-core configurations, which are not considered in this paper. The squares of the coefficients in this expansion are the spectroscopic factors; in particular, the square of the coefficient of the single-particle term is just the spectroscopic factor that would be deduced from a (d,p) experiment on the same target.

Auerbach and Stein[15] have performed weak-coupling model calculations for these states in ^{207}Pb, using only the terms shown explicitly in Eq. (1). Their theoretical predictions can be compared directly to our experimental results.

 ©1983 The American Physical Society

When such a comparison is made, significant discrepancies are seen between experiment and theory, indicating that additional weak-coupling model calculations, using a larger basis than that used by Auerbach and Stein, are needed to explain the structure of these states.

II. EXPERIMENT

The measurements described in this paper were made using the University of Washington FN tandem Van de Graaff accelerator, with a polarized proton beam which was produced by a Lamb-shift polarized ion source. Typical beam currents were 45–85 nA, with an average polarization of 70–75%. The beam was focused through a 3-mm diam defining aperture before passing through the target and the helium polarimeter and being collected by the Faraday cup. The scattered particles were detected by silicon surface-barrier detectors at $\theta_{lab}=120°$, 135°, 150°, and 165° (all on the right-hand side of the beam), and by a monitor detector at $\theta_{lab}=35°$ (on the left-hand side of the beam). Each of these had a thickness of at least 2 mm (the range of 18-MeV protons in silicon). The back-angle detectors were 20 cm from the target (17.5 cm for some early runs), and had solid angles ranging from 1.5 to 3.4 msr. Shielding and magnetic electron suppression were used to reduce the background in the back-angle spectra.

The target consisted of a self-supporting foil of isotopically enriched (97.2%) ^{206}Pb.[16] It was mounted at an angle of 25° from the normal to the beam direction in order to minimize the total energy loss in the target for elastically scattered protons. The effective thickness was approximately 1.1 mg/cm^2, corresponding to an energy loss of 15 keV at $E_p=16$ MeV. This was small compared to the widths of the observed IAR's (>200 keV) and to the energy spacing between data points (50 keV).

The polarimeter consisted of a cylindrical gas cell, 3.8 cm in diameter and filled with one atmosphere of helium, and two symmetrically placed Si(Li) detectors at $\theta_{lab}=112°$, each located 15.4 cm from the center of the cell.

At each proton energy, data were taken for both "spin up" and "spin down." The spin direction was controlled by small transverse-field coils in the crossover region of the ion source[17]; when the coils were turned on, the spin was rotated through 180°. This spin rotation process caused some depolarization, so the spin-up polarization (p_+) was about 5–10% greater than the spin-down polarization (p_-). However, none of the other properties of the beam, such as intensity, emittance, or position, was affected by the rotation. For about half of the energies, the data were taken in separate spin-up and spin-down runs; for the others, the spin was flipped every 100 ms, so that the data for both spin states could be collected during a single run.

A typical pulse-height spectrum for a back-angle detector is shown in Fig. 1. For all of the energies and angles of interest, the first excited state (2$^+$, 0.803 MeV) was well separated from the other ^{206}Pb peaks and from the contaminant peaks. The background was quite low and was assumed to be a constant for all energies below the elastic peak. In almost all cases the assumed background under a peak of interest was less than the statistical error in the peak area.

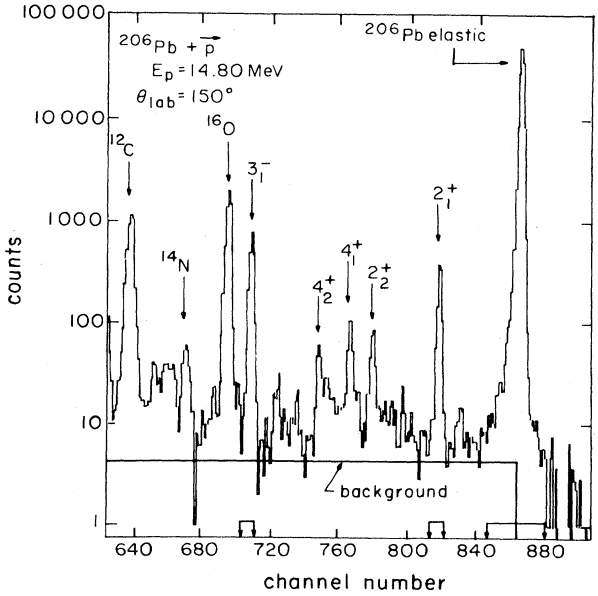

FIG. 1. Energy spectrum for ^{206}Pb+$\vec{p}$ at $E_p=14.80$ MeV, $\theta_{lab}=150°$, spin up. The brackets on the horizontal axis indicate the windows used to determine the peak areas.

The fact that p_+ and p_- were different was taken into account in calculating the cross sections and analyzing powers.[18] We were able, by taking appropriate combinations of the polarimeter yields, to determine p_+ and p_- separately, as well as the average polarization $p_0\equiv\frac{1}{2}(p_++p_-)$. Then, since the integrated beam currents for the two spin states (Q_+ and Q_-) were equal, the cross sections $\sigma(\theta)$ and analyzing powers $A_y(\theta)$ for the back-angle detectors were given by

$$\sigma(\theta)=\frac{p_-Y_+(\theta)+p_+Y_-(\theta)}{2p_0Q_+\Omega(\theta)\beta} \tag{2}$$

and

$$A_y(\theta)=\frac{Y_-(\theta)-Y_+(\theta)}{p_-Y_+(\theta)+p_+Y_-(\theta)}\ , \tag{3}$$

where $Y_+(\theta)$ and $Y_-(\theta)$ are the spin-up and spin-down peak areas, $\Omega(\theta)$ is the detector solid angle, and β is an overall normalization constant which is proportional to the target thickness. The same expressions were used for the monitor, except that the sign of $A_y(\theta)$ was the opposite of that shown in Eq. (3), since the detector was on the opposite side of the beam. The values of the normalization constants $\Omega(\theta)$ and β were determined by measuring the yields at low energies ($E_p=4$, 6, 8, 10, 12, and 13.75 MeV) and comparing them with optical-model predictions; this procedure is described in detail in Ref. 18. The value of Q_+ for each polarized-beam run was then found by using Eq. (2), with the monitor yields and the monitor cross section given as inputs (the cross sections were measured in a separate series of short unpolarized-beam runs). This nor-

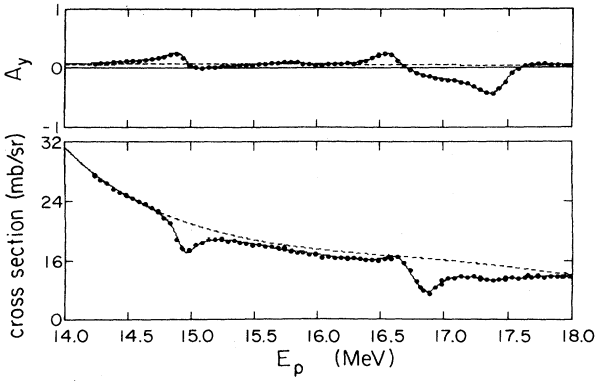

FIG. 2. Differential cross sections and analyzing powers for ^{206}Pb($\vec{p}$,p$_0$) at $\theta_{lab}=120°$. The solid curves show the best fit using isobaric analog resonances and parametrized background; the dashed curves give the results using only the background.

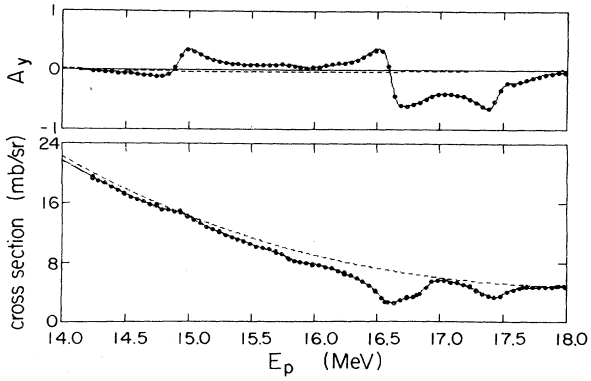

FIG. 4. Differential cross sections and analyzing powers for ^{206}Pb($\vec{p}$,p$_0$) at $\theta_{lab}=150°$. The solid curves show the best fit using isobaric analog resonances and parametrized background; the dashed curves give the results using only the background.

malization process produced an uncertainty of about 0.9% in each of the values of $\sigma(\theta)$, in addition to the statistical error. There was also an overall normalization error of about 0.75% because of the uncertainty in the low-energy monitor cross sections.

The experimental results are shown in Figs. 2–5 for the elastic scattering and in Figs. 6–9 for the inelastic scattering to the 2^+ (0.803 MeV) state. The cross sections and analyzing powers were measured between $E_p=14.25$ and 18.00 MeV in increments of 50 keV. In addition to the excitation functions shown here, there were also some partial angular distributions, which were obtained by taking data at four additional angles at $E_p=13.75$, 15.50, and 18.00 MeV.

III. ANALYSIS OF ELASTIC SCATTERING DATA

A. Method of analysis

The theoretical cross sections and analyzing powers for the elastic scattering of protons from a spin-zero target can be written as[19]

$$\sigma^{\rm th}(E,\theta)=|A(E,\theta)|^2+|B(E,\theta)|^2$$

and

$$\sigma^{\rm th}(E,\theta)A_y^{\rm th}(E,\theta)=2\,{\rm Re}[A(E,\theta)B(E,\theta)^*]\,,$$

where the scattering amplitudes $A(E,\theta)$ and $B(E,\theta)$ are given by the partial wave expansions

$$A(E,\theta)=f_C(E,\theta)+\frac{1}{2ik}\sum_{l=0}^{\infty}\sum_{j=l-1/2}^{l+1/2}(j+\tfrac{1}{2})e^{2i\sigma_l}(S_{lj}-1)P_l(\cos\theta)$$

and

$$B(E,\theta)=\frac{1}{2k}\sum_{l=0}^{\infty}\sum_{j=l-1/2}^{l+1/2}(-1)^{j-l-1/2}e^{2i\sigma_l}S_{lj}P_l^1(\cos\theta)\,.$$

In these expressions, $f_C(E,\theta)$ is the Coulomb scattering amplitude,

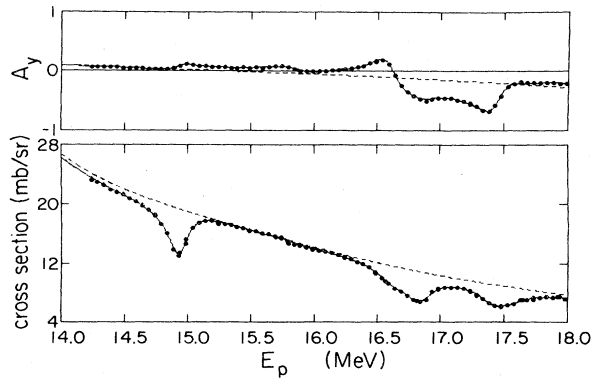

FIG. 3. Differential cross sections and analyzing powers for ^{206}Pb($\vec{p}$,p$_0$) at $\theta_{lab}=135°$. The solid curves show the best fit using isobaric analog resonances and parametrized background; the dashed curves give the results using only the background.

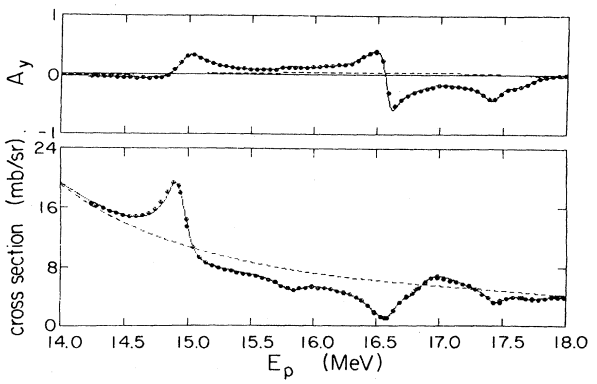

FIG. 5. Differential cross sections and analyzing powers for ^{206}Pb($\vec{p}$,p$_0$) at $\theta_{lab}=165°$. The solid curves show the best fit using isobaric analog resonances and parametrized background; the dashed curves give the results using only the background.

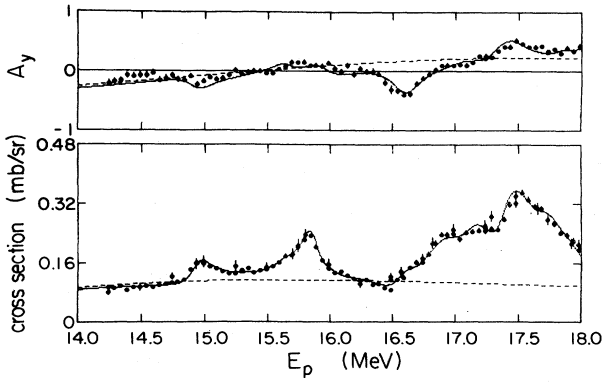

FIG. 6. Differential cross sections and analyzing powers for proton inelastic scattering to the 2^+ (0.803 MeV) state of ^{206}Pb at $\theta_{lab}=120°$. The solid curves indicate the best fit; the dashed curves show the DWBA background.

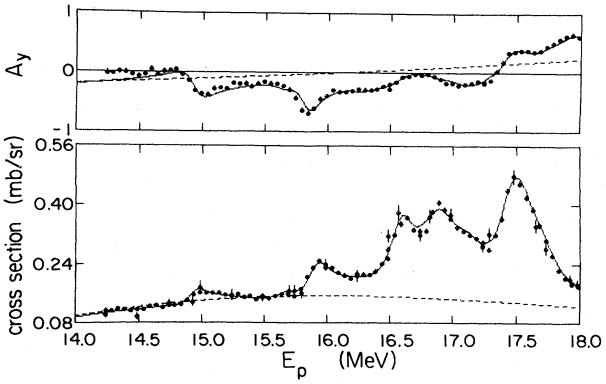

FIG. 8. Differential cross sections and analyzing powers for proton inelastic scattering to the 2^+ (0.803 MeV) state of ^{206}Pb at $\theta_{lab}=150°$. The solid curves indicate the best fit; the dashed curves show the DWBA background.

$$f_C(E,\theta)=-\frac{\eta}{2k\sin^2(\frac{1}{2}\theta)}\exp\{-i\eta\ln[\sin^2(\tfrac{1}{2}\theta)]+2i\sigma_0\}\ ,$$

σ_l is the Coulomb phase shift,

$$\sigma_l=\arg\Gamma(l+1+i\eta)\ ,$$

and S_{lj} is the scattering matrix (S-matrix) element. Also, $\eta=\mu Ze^2/(\hbar^2k)$, $k=(2\mu E)^{1/2}/\hbar$, μ is the reduced mass, Z is the atomic number of the target, and θ and E are the scattering angle and bombarding energy, respectively, in the center-of-mass system. Compound elastic scattering has been neglected because of the large number of open channels at the energies of interest.

The S-matrix element S_{lj} in the vicinity of isobaric analog resonances can be written as the sum of a resonant and a nonresonant ("background") part,[12]

$$S_{lj}=S_{lj}^R+S_{lj}^B\ ,$$

where the nonresonant part is expressed in terms of the nuclear phase shift,

$$S_{lj}^B=\exp[2i(\delta_{lj}+i\eta_{lj})]\ ,$$

and the resonant part is assumed to be a sum of independent contributions from all of the resonances which have the appropriate spin and parity,

$$S_{lj}^R=-i\sum_\lambda\frac{\Gamma_{lj}^\lambda\exp[2i(\delta_{lj}+\phi_{lj}^\lambda)]}{E-E_\lambda+\frac{1}{2}i\Gamma_\lambda}\ . \tag{4}$$

The index λ is used here to identify a particular IAR, which is characterized by its center-of-mass energy E_λ, its total width Γ_λ, its elastic partial width Γ_{lj}^λ, and its elastic resonance mixing phase ϕ_{lj}^λ. It should be emphasized that Eq. (4) is only a plausible assumption; the current theories of IAR's deal with isolated resonances and do not specify what corrections, if any, are required in the case of overlapping resonances with the same spin and parity.

The scattering amplitudes $A(E,\theta)$ and $B(E,\theta)$ can also be written, in an obvious way, as sums of resonant and nonresonant parts. In order to fit the excitation-function data, we had to calculate the nonresonant amplitudes

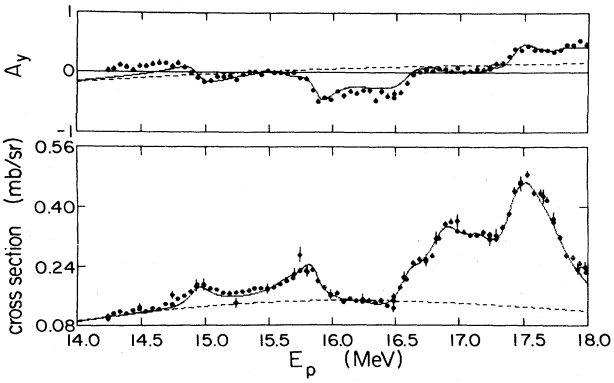

FIG. 7. Differential cross sections and analyzing powers for proton inelastic scattering to the 2^+ (0.803 MeV) state of ^{206}Pb at $\theta_{lab}=135°$. The solid curves indicate the best fit; the dashed curves show the DWBA background.

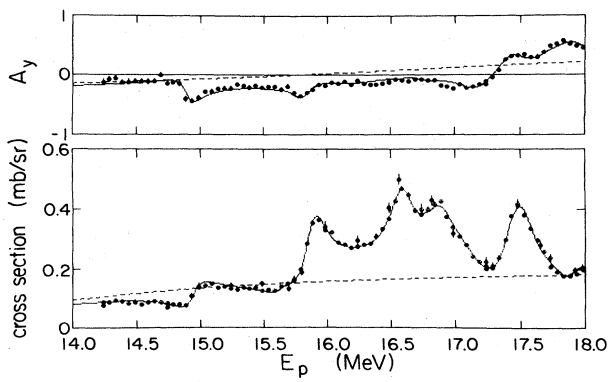

FIG. 9. Differential cross sections and analyzing powers for proton inelastic scattering to the 2^+ (0.803 MeV) state of ^{206}Pb at $\theta_{lab}=165°$. The solid curves indicate the best fit; the dashed curves show the DWBA background.

$A_B(E,\theta)$ and $B_B(E,\theta)$ and vary them to fit the off-resonance data. This was done by parametrizing the amplitudes themselves, rather than by using the optical model or varying the phase shifts. That made it possible for us to obtain reasonable resonance parameters, even for the weaker IAR's, without the systematic errors that can be produced when the resonant amplitudes have to compensate for incorrect background amplitudes. Since the nonresonant amplitudes are smoothly varying functions of energy, they were expressed as Taylor-series expansions about the midpoint of the energy range of interest; for $A_B(E,\theta)$ the Taylor series was then multiplied by E^{-1} in order to account for the energy dependence of the Coulomb scattering amplitude. A separate set of expansion coefficients was used for each of the four angles. In addition, each of the amplitudes was multiplied by a phase factor in order to make $A_B(E,\theta)$ real; this reduced the number of background parameters and eliminated an arbitrary phase, but it also caused the resonance mixing phase ϕ_{lj}^{λ} for each IAR to be replaced by a set of phases $\tilde{\phi}_{lj}^{\lambda}(\theta)$, so that this method could not be used to find ϕ_{lj}^{λ}.

The parametrized-background approach was used in the fitting program IAR4. This program calculated the theoretical cross sections $\sigma^{\text{th}}(E,\theta)$ and analyzing powers $A_y^{\text{th}}(E,\theta)$ for each energy at which the corresponding experimental quantities $\sigma^{\text{ex}}(E,\theta)$ and $A_y^{\text{ex}}(E,\theta)$ were available; it then varied selected background and/or resonance parameters in order to minimize the quantity

$$\chi_\nu^2=\frac{1}{\nu}(\chi_p^2+\chi_\sigma^2)\ ,$$

where

$$\chi_p^2=\sum_{E,\theta}\left[\frac{A_y^{\text{ex}}(E,\theta)-A_y^{\text{th}}(E,\theta)}{\delta A_y^{\text{ex}}(E,\theta)}\right]^2$$

and

$$\chi_\sigma^2=\sum_{E,\theta}\left[\frac{\sigma^{\text{ex}}(E,\theta)-\sigma^{\text{th}}(E,\theta)}{\delta\sigma^{\text{ex}}(E,\theta)}\right]^2 .$$

In these expressions, $\delta A_y^{\text{ex}}(E,\theta)$ and $\delta\sigma^{\text{ex}}(E,\theta)$ are the experimental errors and ν is the number of degrees of freedom. One very useful feature of IAR4 was its ability to "link" two or more resonance parameters together so that they maintained a fixed relationship to each other as they varied.[20] Thus, if two of the Γ_{lj}^{λ}'s or two of the Γ_λ's were linked together, then their ratio remained fixed, while if two of the E_λ's or two of the $\tilde{\phi}_{lj}^{\lambda}(\theta)$'s were linked together, their difference remained fixed. This feature had to be used extensively during the search because of the large number of overlapping IAR's.

The IAR's which were seen in this experiment are the analogs of parent states in ^{207}Pb having excitation energies between about 1.9 and 5.9 MeV. The level structure in that energy range is very complicated; a large number of states have been observed there in ^{206}Pb(d,p),[21] ^{206}Pb(d,pγ),[22] ^{207}Pb(p,p'),[23] ^{207}Pb(γ,γ'),[24,25] and ^{208}Pb(d,t).[21] Since different reactions tend to populate different types of states, it is difficult to correlate the results of these experiments so as to obtain a unified level structure. Therefore, what we did for the analysis of the present experiment was to use only those parent states which were excited most strongly in ^{206}Pb(d,p), since these should be the states whose IAR's have the largest elastic partial widths.

The most recent (d,p) results are those of Moyer, Cohen, and Diehl (MCD).[21] Using 17-MeV deuterons, they observed a total of 35 states in the region of interest with maximum cross sections of at least 50 μb/sr. Unfortunately, they were not able to make unambiguous spin assignments for all of those states on the basis of their DWBA analysis. In fact, in many cases they were not even able to distinguish between different values of the orbital angular momentum. The determination of the l and j values for these states was thus an important part of the analysis of our data.

Many of the resonance parameters were linked together during the search, in order to reduce the number of variable parameters and to ensure that the results would be physically reasonable. For example, the resonance energies E_λ were all linked together, and only the overall energy scale was varied during the fitting process. The differences in the resonance energies of the IAR's were required to be the same as the differences in the excitation energies of the corresponding parent states. Also, the values of Γ_{lj}^{λ} for all the IAR's with the same l and j were linked together. For each such pair of IAR's, the ratio of the partial widths was given by the ratio of the (d,p) spectroscopic factors, multiplied by the ratio of the single-particle widths. The spectroscopic factors for some of the parent states were given explicitly by MCD; for the others, they had to be inferred from the measured (d,p) cross sections and from the spectroscopic factors of nearby states. The single-particle widths were calculated by the program ANALOG (discussed below), using optical-model parameters[18] which described the elastic scattering from ^{208}Pb (the ratios of these widths turned out to be nearly identical to those calculated later using ^{206}Pb optical-model parameters). ANALOG was also used to estimate the differences between the values of $\tilde{\phi}_{lj}^{\lambda}(\theta)$ for pairs of IAR's with the same l and j, and these differences remained fixed during the fitting process. Finally, the total widths Γ_λ were assumed to be the same for all IAR's having the same l and j. This assumption seemed plausible, since Γ_λ is a monotonic function of l for the IAR's in ^{209}Bi.[8]

The fit to the excitation functions was done in stages, with more resonances being included at each stage. Initially, only 15 IAR's were used, corresponding to the 15 strongest states in ^{207}Pb [i.e., those with the largest maximum (d,p) cross sections]. States were then added in order of decreasing strength until a total of 35 IAR's was included. We decided to stop at that point, since the next strongest state was 30% weaker than the last one that we used, and since the last few states had produced only marginal changes in the fit. At each stage, we were able to obtain a reasonably good fit to the excitation functions by using appropriate spin-parity assignments and varying the resonance parameters.

TABLE I. Spins and parities for states in ^{207}Pb. For each state, the spin assignment and the basis for making it are given, along with the assignments made by previous authors. An asterisk indicates that the level was observed, but that no spin assignment was made.

Level	E_x[a] (MeV)	Present work J^π	Basis[b]	Previous work (d,p)[a]	(d,pγ)[c]	(p,p′)[d]	(γ,γ′)[e]	Compilation[f]
1	2.339	$\frac{7}{2}^-$	(1)	$(\frac{7}{2}^-)$	$\frac{7}{2}^-$	$\frac{7}{2}^-, \frac{9}{2}^-$		$\frac{7}{2}^-$
2	2.624	$\frac{5}{2}^+$	(1)	*	$\frac{5}{2}^+$	$\frac{5}{2}^+, \frac{7}{2}^+$		$\frac{5}{2}^+$
3	2.728	$\frac{9}{2}^+$	(1)	$\frac{9}{2}^+$	$\frac{9}{2}^+$	$\frac{9}{2}^+, \frac{11}{2}^+$		$\frac{9}{2}^+$
4	3.430	$\frac{9}{2}^+$	(2)	*		$(\frac{9}{2}^+, \frac{11}{2}^+)$		$(\frac{9}{2}^+, \frac{11}{2}^+)$
5	3.510	$\frac{11}{2}^+$	(1)	$\frac{11}{2}^+(\frac{15}{2}^-)$		$(\frac{9}{2}^+, \frac{11}{2}^+)$		$(\frac{11}{2}^+)$
6	3.620	$\frac{11}{2}^+$	(2)	*		$\frac{9}{2}^+, \frac{11}{2}^+$		$(\frac{9}{2}^+, \frac{11}{2}^+)$
7	3.635	$\frac{5}{2}^+$	(1)	$\frac{5}{2}^+$	$(\frac{5}{2}^+)$	$\frac{5}{2}^+, \frac{7}{2}^+$		$\frac{5}{2}^+$
8	3.725	$\frac{5}{2}^+$	(2)	$l=2,3$		*		
9	4.000	$\frac{5}{2}^+$	(2)	$l=2,3$		*		
10	4.115	$\frac{15}{2}^-$	(1)	$\frac{15}{2}^-(\frac{11}{2}^+)$				$(\frac{15}{2}^-)$
11	4.319	$\frac{5}{2}^+$	(1)	$\frac{5}{2}^+$	$(\frac{5}{2}^+)$			$(\frac{5}{2}^+)$
12	4.389	$\frac{5}{2}^+$	(1)	$\frac{5}{2}^+$	$\frac{5}{2}^+$	*		$\frac{5}{2}^+$
13	4.538	$\frac{1}{2}^+$	(1)	$\frac{1}{2}^+$		*		$(\frac{1}{2}^+)$
14	4.581	$\frac{5}{2}^+$	(1)	$\frac{5}{2}^+(\frac{7}{2}^-)$				
15	4.613	$\frac{5}{2}^+$	(3)	*		*		
16	4.627	$\frac{1}{2}^+$	(1)	$\frac{1}{2}^+$	$\frac{1}{2}^+$	$(\frac{15}{2}^-, \frac{17}{2}^-)$	$(\frac{1}{2}^+)$	$\frac{1}{2}^+$
17	4.641	$\frac{1}{2}^+$	(3)	*				
18	4.871	$\frac{7}{2}^+$	(2)	$\frac{5}{2}^+, \frac{7}{2}^-, \frac{7}{2}^+$		*	$(\frac{1}{2}^+, \frac{3}{2}^+)$	$(\frac{3}{2}^+)$
19	4.985	$\frac{1}{2}^+$	(1)	$\frac{1}{2}^+$		$\frac{5}{2}^+, \frac{7}{2}^+$	$(\frac{1}{2}^+, \frac{3}{2}^+)$	$(\frac{1}{2}^+)$
20	5.057	$\frac{7}{2}^+$	(3)	$l=4,2,3$		*		
21	5.072	$\frac{3}{2}^+$	(3)	*				
22	5.080	$\frac{3}{2}^+$	(2)	$l=4,2,3$		$\frac{5}{2}^+, \frac{7}{2}^+$		$(\frac{5}{2}^+, \frac{7}{2}^+)$
23	5.130	$\frac{3}{2}^+$	(2)	$\frac{7}{2}^+$	*	*		
24	5.181	$\frac{7}{2}^+$	(2)	$\frac{3}{2}^+$	*	$\frac{5}{2}^+, \frac{7}{2}^+$		$(\frac{7}{2}^+)$
25	5.205	$\frac{3}{2}^+$	(1)	$l=4,2,3$	$\frac{3}{2}^+$		*	
26	5.219	$\frac{3}{2}^+$	(1)	$\frac{3}{2}^+$		*	*	$(\frac{3}{2}^+)$
27	5.269	$\frac{7}{2}^+$	(3)	*		$\frac{5}{2}^+, \frac{7}{2}^+$		$(\frac{5}{2}^+, \frac{7}{2}^+)$
28	5.313	$\frac{7}{2}^+$	(2)	$\frac{7}{2}^+, \frac{3}{2}$		*		
29	5.370	$\frac{7}{2}^+$	(3)	*		$(\frac{11}{2}^-, \frac{13}{2}^-)$		
30	5.432	$\frac{7}{2}^+$	(2)	$\frac{7}{2}^+, \frac{3}{2}^+$		$\frac{5}{2}^+, \frac{7}{2}^+$		$(\frac{5}{2}^+, \frac{7}{2}^+)$
31	5.493	$\frac{3}{2}^+$	(3)	*			$(\frac{1}{2}^+, \frac{3}{2}^+)$	
32	5.503	$\frac{3}{2}^+$	(2)	*		$\frac{7}{2}^-, \frac{9}{2}^-$		$(\frac{7}{2}^-, \frac{9}{2}^-)$
33	5.575	$\frac{3}{2}^+$	(2)	$\frac{3}{2}^+, \frac{7}{2}^-, \frac{7}{2}^+$				
34	5.618	$\frac{7}{2}^+$	(2)	*		$(\frac{5}{2}^+, \frac{7}{2}^+)$		
35	5.692	$\frac{3}{2}^+$	(2)	$\frac{7}{2}^+, \frac{3}{2}^+$		*	$(\frac{1}{2}^+, \frac{3}{2}^+)$	

[a]Reference 21.

[b]Basis for spin assignment: (1) taken from the literature; was consistent with the present data. (2) preferred; clearly gave the best fit to the present data. (3) tentative; gave slightly better fit than alternative assignments.

[c]Reference 22.

[d]Reference 23.

[e]References 24 and 25.

[f]*Table of Isotopes*, 7th ed., edited by C. M. Lederer and V. S. Shirley (Wiley, New York, 1978).

B. Results

The spins and parities that were used for the IAR's of the 35 parent states in ^{207}Pb are shown in Table I. Also shown in the table are the spin-parity assignments given by previous authors for the same states (or, in some cases, for other states having nearly the same energy). For each state, the table indicates the basis for our assignment. Where there was a consensus in the literature, we used the accepted spin-parity assignment, provided it gave a reasonably good fit to our data. Where there was no consensus, we tried several different assignments and chose the one which gave the best fit. In some cases, this procedure clearly favored a particular spin assignment; in other cases, however, the difference in χ_ν^2 was too small for anything more than a tentative assignment to be made. Each level for which we have made a new and/or different spin assignment is discussed in detail below.

Levels 4 ($E_x=3.430$ MeV) and 6 ($E_x=3.620$ MeV) are excited by $l=5$ transitions in ^{207}Pb(p,p'),[23] so each level might have been either $\frac{9}{2}^+$ or $\frac{11}{2}^+$. Our data, however, clearly required a $\frac{9}{2}^+$ assignment for level 4 and an $\frac{11}{2}^+$ for level 6; each of the other three combinations gave a worse fit.

Levels 8 ($E_x=3.725$ MeV) and 9 ($E_x=4.000$ MeV) were identified only as $l=2,3$ by MCD. The $l=3$ assignment seemed implausible, however, since a $\frac{5}{2}^-$ or $\frac{7}{2}^-$ state could be formed in ^{206}Pb(d,p)^{207}Pb only by filling one of the two holes in the $82<N\leq 126$ neutron shell; such a state would also be strongly excited in a neutron pickup reaction, contrary to what was observed by MCD in ^{208}Pb(d,t)^{207}Pb. Another possibility, suggested by Ayoub, Ascuitto, and Bromley,[26] was that level 8 was the weak $g_{9/2}$ state predicted by Auerbach and Stein.[15] Therefore, both $\frac{5}{2}^+$ and $\frac{9}{2}^+$ were tried for each of these two levels, with $\frac{5}{2}^+$ giving a much better fit in each case.

Level 14 ($E_x=4.581$ MeV) has been seen only by MCD, who gave it a $\frac{5}{2}^+$ assignment, with $\frac{7}{2}^-$ as a possible alternative. We assumed that the $\frac{5}{2}^+$ assignment was correct, and did not check any other possibilities.

Levels 15 ($E_x=4.613$ MeV) and 17 ($E_x=4.641$ MeV) are very close to a much stronger state (level 16, $E_x=4.627$ MeV), so their (d,p) angular distributions could not be analyzed by MCD. The fit to our data was slightly better with the assignments given in Table I than it was with any other combination of $\frac{5}{2}^+$ and $\frac{1}{2}^+$ assignments, but the choice was by no means clear. The fact that level 15 ($\frac{5}{2}^+$) was seen in ^{207}Pb(p,p') while level 17 ($\frac{1}{2}^+$) was not seen gives some additional support to our choice, since (p,p') excites mostly the higher spin states.

Level 18 ($E_x=4.871$ MeV) may actually be a pair of nearly degenerate levels, a $\frac{3}{2}^+$ (or $\frac{1}{2}^+$) which is strongly excited in (γ,γ') (Refs. 24 and 25) and a $\frac{7}{2}^+$ (or $\frac{5}{2}^+$) which is populated in (d,p) and possibly in (p,p'). The $\frac{7}{2}^+$ assignment which is given here produced a considerably better fit to our data than did either the $\frac{3}{2}^+$ or $\frac{5}{2}^+$.

The assignments for levels 20 ($E_x=5.057$ MeV), 21 ($E_x=5.072$ MeV), and 22 ($E_x=5.080$ MeV) are somewhat tentative. The set of spin assignments given in Table I ($\frac{7}{2}^+,\frac{3}{2}^+,\frac{3}{2}^+$) produced the best fit; however, there was an alternative set ($\frac{3}{2}^+,\frac{7}{2}^+,\frac{3}{2}^+$) which was almost as good and cannot be ruled out. Note that our $\frac{3}{2}^+$ assignment for level 22 is not consistent with the (p,p') results.

The assignments for the two strong states at $E_x=5.130$ MeV (level 23, $\frac{3}{2}^+$) and 5.181 MeV (level 24, $\frac{7}{2}^+$) were clearly required by our data, even though they are exactly the opposite of those made by MCD. However, our assignments are not inconsistent with MCD's experimental (d,p) angular distributions, since each of those is fitted almost equally well by both the $d_{3/2}$ and $g_{7/2}$ DWBA curves. The present results are supported by Wagner, Crawley, and Hammerstein (WCH),[23] who gave an $l=3$ assignment (i.e., $\frac{5}{2}^+$ or $\frac{7}{2}^+$) to level 24 on the basis of their (p,p') data.

It was not possible to decide on the basis of our data between $\frac{3}{2}^+$ and $\frac{7}{2}^+$ for level 25 ($E_x=5.205$ MeV), since the fit was equally good for either choice. Therefore, the $\frac{3}{2}^+$ assignment for this state was taken from the (d,pγ) results[22]; this choice was also supported by the presence of a level at about the same energy in (γ,γ') (which excites mostly the lower spin states).

For level 27 ($E_x=5.269$ MeV), the fit was somewhat better with $\frac{7}{2}^+$ than with $\frac{3}{2}^+$, in agreement with the $l=3$ assignment of WCH.

The strong state at $E_x=5.313$ MeV (level 28) has a definite assignment of $\frac{7}{2}^+$, with $\frac{3}{2}^+$ producing a qualitatively worse fit to our data. This is also the case for the somewhat weaker level 30 ($E_x=5.432$ MeV).

Level 29 ($E_x=5.370$ MeV) was the only state with $E_x>5$ MeV for which an assignment other than $\frac{3}{2}^+$ or $\frac{7}{2}^+$ was attempted. Since there is a level at this energy which WCH tentatively identified as $\frac{11}{2}^-$ or $\frac{13}{2}^-$, and since there is also a weak $\frac{11}{2}^-$ IAR in ^{209}Bi at about the same bombarding energy,[18] we decided to try the $\frac{11}{2}^-$ assignment in addition to the $\frac{3}{2}^+$ and $\frac{7}{2}^+$. However, it was the $\frac{7}{2}^+$ assignment which gave the best fit to our data, with $\frac{11}{2}^-$ and $\frac{3}{2}^+$ each producing somewhat worse results.

Of the five remaining levels, the strongest two, levels 32 ($E_x=5.503$ MeV) and 33 ($E_x=5.575$ MeV), were tested first. The best fit was obtained when both of them were assumed to be $\frac{3}{2}^+$; each of the other three combinations of $\frac{7}{2}^+$ and $\frac{3}{2}^+$ assignments was clearly worse. These states have not been observed in either (p,p') or (γ,γ'); the $l=4$ state which was seen in (p,p') at $E_x=5.501$ MeV is not the same as level 32, since it is not excited in ^{208}Pb(d,t).

Levels 31 ($E_x=5.493$ MeV) and 34 ($E_x=5.618$ MeV) were tested next, using the four possible combinations of $\frac{7}{2}^+$ and $\frac{3}{2}^+$ assignments. The data clearly favored $\frac{7}{2}^+$ for level 34, in agreement with the tentative $l=3$ assignment given by WCH. For level 31, however, the evidence for our $\frac{3}{2}^+$ assignment was considerably weaker. The fact that a dipole state was observed in (γ,γ') at $E_x=5.489$ MeV tends to support our choice of $\frac{3}{2}^+$ for this level.

Finally, for level 35 ($E_x=5.692$ MeV), the $\frac{3}{2}^+$ assignment produced a noticeably better fit than did the $\frac{7}{2}^+$. This level is probably the same as the dipole state which was seen in (γ,γ') at $E_x=5.690$ MeV.

Once all of the spin assignments had been determined,

TABLE II. Resonance parameters for the isobaric analog resonances of 35 states in ^{207}Pb. Whenever a number in parentheses is given instead of an uncertainty, it means that that parameter was linked to the corresponding parameter for a different level (indicated by the number in parentheses).

Level	E_λ[a] (MeV)	J^π	Γ_λ (keV)	Γ_{lj}^λ (keV)	ϕ_{lj}^λ (deg)
1	14.471	$\frac{7}{2}^-$	286[b]	0.52[b]	22.5[b]
2	14.756	$\frac{5}{2}^+$	211(7)	0.15(7)	7.5(7)
3	14.860	$\frac{9}{2}^+$	195±3	19.44±0.27	2.3±0.3
4	15.562	$\frac{9}{2}^+$	195(3)	0.66(3)	2.8(3)
5	15.642	$\frac{11}{2}^+$	266±19	1.25±0.08	−1.3±2.9
6	15.752	$\frac{11}{2}^+$	266(5)	1.10(5)	−1.2(5)
7	15.767	$\frac{5}{2}^+$	211±12	4.17±0.21	5.5±0.8
8	15.857	$\frac{5}{2}^+$	211(7)	0.81(7)	5.3(7)
9	16.132	$\frac{5}{2}^+$	241(12)	0.68(12)	6.5(11)
10	16.247	$\frac{15}{2}^-$	266(5)	1.03±0.14	−26.9±5.0
11	16.451	$\frac{5}{2}^+$	241±22	6.70(12)	5.7±3.7
12	16.521	$\frac{5}{2}^+$	227±5	27.32±0.59	−5.5±0.9
13	16.670	$\frac{1}{2}^+$	295(16)	3.72(16)	0.4(16)
14	16.713	$\frac{5}{2}^+$	227(12)	0.83(12)	−6.1(12)
15	16.745	$\frac{5}{2}^+$	227(12)	0.62(12)	−6.2(12)
16	16.759	$\frac{1}{2}^+$	295±8	47.79±1.40	0.0±0.4
17	16.773	$\frac{1}{2}^+$	295(16)	3.37(16)	0.0(16)
18	17.003	$\frac{7}{2}^+$	257(24)	1.84±0.20	2.9(24)
19	17.117	$\frac{1}{2}^+$	295(16)	4.16(16)	−1.6(16)
20	17.189	$\frac{7}{2}^+$	257(24)	1.48(24)	2.7(24)
21	17.204	$\frac{3}{2}^+$	260(26)	1.40(26)	18.9(23)
22	17.212	$\frac{3}{2}^+$	260(26)	1.82(26)	18.9(23)
23	17.262	$\frac{3}{2}^+$	260(26)	5.55(26)	18.7±1.9
24	17.313	$\frac{7}{2}^+$	257±11	14.29±0.68	2.5±0.9
25	17.337	$\frac{3}{2}^+$	260(26)	4.28(26)	−1.9(26)
26	17.351	$\frac{3}{2}^+$	260±5	32.40±0.76	−2.0±0.4
27	17.401	$\frac{7}{2}^+$	284(28)	1.05(28)	0.0(28)
28	17.445	$\frac{7}{2}^+$	284±27	4.62±0.34	0.0±1.4
29	17.502	$\frac{7}{2}^+$	284(28)	1.33(28)	−0.1(28)
30	17.564	$\frac{7}{2}^+$	284(28)	3.69(28)	−0.2(28)
31	17.625	$\frac{3}{2}^+$	260(26)	1.04(26)	−4.5(33)
32	17.635	$\frac{3}{2}^+$	260(26)	1.90(26)	−4.6(33)
33	17.707	$\frac{3}{2}^+$	260(26)	2.33(26)	−4.9±1.3
34	17.750	$\frac{7}{2}^+$	284(28)	1.11(28)	−0.5(28)
35	17.824	$\frac{3}{2}^+$	260(26)	0.92(26)	−5.3(33)

[a]The overall uncertainty in the energy scale is 0.001 MeV.
[b]Not varied.

an attempt was made to remove some of the constraints on the values of Γ_λ, Γ_{lj}^λ, and $\tilde{\phi}_{lj}^\lambda(\theta)$. However, it was not possible to do this in more than a few cases without getting unreasonable results. Therefore, the best-fit resonance parameters shown in Table II are not all independent; most of them belong to groups of parameters which were linked together throughout the fitting process. Within each group an error is given only for the strongest

resonance; it indicates the uncertainty in that one parameter when all the other parameters in the group are varied along with it.

The best fit to the elastic scattering data is shown by the solid curves in Figs. 2–5. The quality of the fit is very good for both the cross sections and the analyzing powers. The good fit to the analyzing-power data is particularly significant, since it provides a strong argument for the correctness of the spin assignments made in this paper. The dashed curves that are also shown in these figures are the results of calculations using the same background as for the solid curves, but without the contributions from the resonances.

After the parametrized-background analysis had been completed, the elastic scattering data were reanalyzed, this time using the optical model to compute the nonresonant amplitudes. There were three reasons for doing this: (1) it allowed us to check the results of the IAR4 analysis; (2) it gave the resonance mixing phases ϕ_{lj}^{λ} directly; and (3) it produced a consistent set of optical-model parameters which could then be used as input for subsequent calculations.

The optical potential that we used had the standard Becchetti-Greenlees form.[27] The volume imaginary potential (W_v) was fixed at zero, and the Coulomb radius (r_C) was fixed[28] at 1.19 fm; all the other optical-model parameters, including the derivatives with respect to energy of the real and surface imaginary potentials (V_R and W_{SF}), were allowed to vary. Also, the resonance parameters E_λ, Γ_λ, and Γ_{lj}^{λ} were fixed at the values obtained from the parametrized-background search, so that only the resonance mixing phases (ϕ_{lj}^{λ}) were allowed to vary. As before, the phases for IAR's with the same spin and parity were linked together, with the differences in the values of ϕ_{lj}^{λ} within each group being obtained from the ANALOG calculations. Two computer programs were used for this reanalysis; one of them (GENOAB) varied the optical-model parameters to fit the angular-distribution data, while the other (RESFIT) varied the resonance parameters to fit the excitation functions.

We were able to achieve the first two goals of the optical-model analysis using "angular distributions" which consisted of the back-angle data points at $E_p = 13.75$, 15.50, and 18.00 MeV. The fits we obtained for the excitation functions were quite good. In fact, they are not even shown in Figs. 2–5 because they were practically indistinguishable from the parametrized-background fits. The best-fit values of the resonance mixing phases are given in Table II, along with the values of E_λ, Γ_λ, and Γ_{lj}^{λ} that were found using IAR4.

To achieve the third goal, which was to find a set of optical-model parameters that could be used in subsequent calculations, it was necessary to consider the forward-angle data points. Those points were not described very well by the parameter set ("set A") that was used to fit the back-angle excitation functions; in particular, the calculated forward-angle oscillations were not as strong as those seen in the data. Therefore, the optical-model parameters were varied again, with the resonance parameters fixed at the values shown in Table II, in order to produce the best fit to all of the angular-distribution data. The resulting parameter set ("set B") is shown in Table III, along with set A and the Becchetti-Greenlees parameter set.[27] Note that in set B the real potential decreases with energy considerably more rapidly than it does in the Becchetti-Greenlees set, and that the surface imaginary potential actually increases with energy instead of decreasing. Both of these results are consistent with previous studies of proton elastic scattering from lead near the Coulomb barrier.[29,30]

IV. ANALYSIS OF INELASTIC SCATTERING DATA

For proton inelastic scattering from a spin-zero target, the theoretical cross sections and analyzing powers are given by[31]

$$\sigma^{\rm th}(E,\theta) = \sum_{\mu_f=-1/2}^{1/2} \sum_{M'=-I'}^{I'} |A(\mu_f,M')|^2$$

and

$$\sigma^{\rm th}(E,\theta)A_y^{\rm th}(E,\theta) = -2\,{\rm Im} \sum_{M'=-I'}^{I'} (-1)^{M'} A(\tfrac{1}{2},M')A(-\tfrac{1}{2},-M')^* \, .$$

In these expressions, I' and M' are the spin and the spin projection, respectively, for the residual nucleus, and μ_f is the spin projection for the outgoing proton. The scattering amplitude $A(\mu_f,M')$ is proportional to the transition matrix (T-matrix) element which describes the inelastic scattering from the initial state (wave vector $=\vec{k}$, proton spin projection $=\frac{1}{2}$) to the final state (wave vector $=\vec{k}'$, residual nucleus spin projection $=M'$, proton spin projection $=\mu_f$),

$$A(\mu_f,M') = \frac{\mu}{2\pi\hbar^2}\left[\frac{k'}{k}\right]^{1/2} \langle \vec{k}',\mu_f,M' \,|\, T \,|\, \vec{k},\tfrac{1}{2}\rangle \, .$$

TABLE III. Optical-model parameters for ^{206}Pb($\vec{p}$,p$_0$). The potentials are in MeV, the radii and diffusenesses are in fm, and ΔV_R ($\equiv -dV_R/dE_p$) and ΔW_{SF} ($\equiv dW_{SF}/dE_p$) are dimensionless. For all three sets, $E_0 = 15.482$ MeV.

Parameter	Present work Set A	Present work Set B	Ref. 27
$V_R(E_0)$	56.99 ±0.96	55.66 ±0.47	59.49
ΔV_R	0.42 ±0.14	0.60 ±0.07	0.32
$W_{SF}(E_0)$	14.37 ±0.79	13.17 ±0.46	10.38
ΔW_{SF}	0.54 ±0.16	0.64 ±0.12	−0.25
V_{so}	8.76 ±0.80	6.80 ±0.41	6.2
r_R	1.249±0.008	1.255±0.006	1.17
r_I	1.210±0.024	1.246±0.008	1.32
r_{so}	1.084±0.017	1.091±0.015	1.01
r_C	1.19	1.19	1.19
a_R	0.647±0.019	0.666±0.009	0.75
a_I	0.564±0.021	0.546±0.013	0.65
a_{so}	0.484±0.069	0.522±0.046	0.75

If E_x is the excitation energy of the residual nucleus, then the magnitude of the exit-channel wave vector is given by $k'=(2\mu E')^{1/2}/\hbar$, where $E'=E-E_x$.

The scattering amplitudes can also be expressed in terms of partial waves. A general partial-wave expansion for both elastic and inelastic scattering, with arbitrary projectile and target spins, is given by Satchler[32]; for the present case, it reduces to

$$A(\mu_f,M')=\frac{1}{2ik}\left[\frac{k'}{k}\right]^{1/2}\sum_{l,j}\sum_{l',j'}(-1)^{j-l-1/2}[4\pi(j+\tfrac{1}{2})]^{1/2}\exp[i(\sigma_l+\sigma'_{l'})]S^{j^\pi}_{I'l'j',0lj}\langle l',\tfrac{1}{2},\tfrac{1}{2}-M'-\mu_f,\mu_f\,|\,j',\tfrac{1}{2}-M'\rangle$$
$$\times\langle I',j',M',\tfrac{1}{2}-M'\,|\,j,\tfrac{1}{2}\rangle Y_{l'}^{-M'+1/2-\mu_f}(\theta,0)\ .$$

The summations over l and j run from 0 to ∞ and from $l-\frac{1}{2}$ to $l+\frac{1}{2}$, respectively; the summations over l' and j', on the other hand, include only those terms permitted by angular momentum conservation, i.e., $|j-I'|\le j'\le j+I'$ and $l'=j'\pm\frac{1}{2}$. Note that the Coulomb phase shifts σ_l and $\sigma'_{l'}$ are evaluated at the entrance- and exit-channel energies, respectively. Note also that the dynamics of the interaction are all contained in the S-matrix element $S^{j^\pi}_{I'l'j',0lj}$, the subscripts of which give the target spin and the proton orbital and total angular momenta, first in the exit channel and then in the entrance channel, and the superscripts of which give the total angular momentum and parity of the system.

We assume that the scattering amplitudes, T-matrix elements, and S-matrix elements can be written as sums of resonant and nonresonant parts[12]; thus, for example,

$$A(\mu_f,M')=A^R(\mu_f,M')+A^B(\mu_f,M')\ . \tag{5}$$

The resonant part of the S matrix is then given by

$$(S^R)^{j^\pi}_{I'l'j',0lj}=-i\sum_\lambda\frac{\gamma^\lambda_{lj}\gamma^\lambda_{l'j'}\exp[i(\delta_{lj}+\delta'_{l'j'}+\phi^\lambda_{lj}+\phi^\lambda_{l'j'})]}{E-E_\lambda+\frac{1}{2}i\Gamma_\lambda}\ . \tag{6}$$

We have introduced here the partial width amplitude γ^λ_{lj}, a real (positive or negative) quantity whose square is the partial width Γ^λ_{lj}. Because of the way in which the partial width amplitudes appear in Eq. (6), there are some ambiguities in their signs. We resolved these ambiguities by using two conventions: (1) all of the entrance-channel amplitudes are positive; and (2) all of the resonance mixing phases are $>-90°$ and $\le+90°$. Note that in Eq. (6) all of the primed quantities refer to the exit channel; in particular, $\delta'_{l'j'}$ is the real part of the exit-channel elastic scattering phase shift. It should be emphasized that some assumptions had to be made in order to write Eqs. (5) and (6). There is no rigorous theoretical justification for splitting the S matrix into independent resonant and nonresonant parts, or for writing the resonant S matrix as a sum of independent contributions from each of the (possibly overlapping) IAR's. Nevertheless, since Eqs. (5) and (6) seem plausible, we have used them to analyze our experimental data, just as previous authors have done.[12,13]

The nonresonant scattering amplitudes $A^B(\mu_f,M')$ were calculated using the distorted-wave Born approximation (DWBA). The distorted waves were generated by solving the Schrödinger equation at both the entrance- and exit-channel energies, using the same spherical optical-model potential that gave the best fit to the elastic scattering angular distributions (set B of Table III). The perturbing potential which connected the initial and final states was then obtained by making a $2^{I'}$-pole deformation in the optical potential; the real, imaginary, spin-orbit, and Coulomb parts of the potential were all deformed equally (the last of these accounted for Coulomb excitation). The strength of the deformation was given by the parameter $\beta_{I'}$, which, for the scattering to the first 2^+ state of ^{206}Pb, has been found by Vallois *et al.*[33] to be $\beta_2=0.048$.

The DWBA calculations were performed using a modified version of Sherif's program HELMY.[31] One of the modifications that we made gave us the option of including nonlocality; to do that, we used the Perey approximation,[34] in which the wave functions are first calculated in the normal way and then damped in the nuclear interior. We also added an option which allowed us to take account of the fact that, because of the energy dependence of the optical potentials, the appropriate values of those potentials were not the same in the entrance and exit channels. However, this option was used only for the real potential; it was assumed that the imaginary potential did not depend on channel energy, but that instead it increased with energy because of the higher level density and greater number of open decay channels at higher compound-nucleus excitation energies.

Figure 10 shows the results of several DWBA calculations at $E_p=13.75$ MeV, an energy at which the effects of the IAR's should be negligible. One of the calculations used a "standard set" of options: Coulomb excitation, no nonlocality, full Thomas form for the spin-orbit deformation,[31] and different real potentials in the entrance and exit channels. The other calculations used other sets of options, with each set differing in only one respect from the standard set. We see that the inclusion of nonlocality (using the 0.85-fm nonlocality length given by Perey and Buck[35]) had little effect, at least at back angles. The calculations with and without nonlocality both described the cross-section data quite well, although neither of them did very well at reproducing the details of the analyzing-power data. The fit to the cross-section data was not quite as good for the other two options (using the same real potential in both entrance and exit channels, and not using Coulomb excitation). The standard set was the one that we decided to use for subsequent calculations.

The program INELAS was used to obtain fits to the inelastic scattering excitation functions. In that program, only the exit-channel partial width amplitudes $\gamma^\lambda_{l'j'}$ and

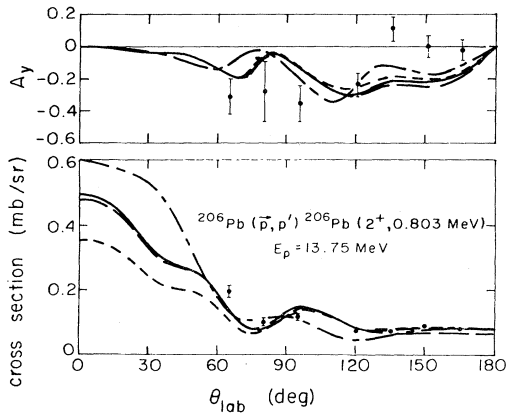

FIG. 10. Differential cross sections and analyzing powers for proton inelastic scattering to the 2^+ (0.803 MeV) state of ^{206}Pb at $E_p = 13.75$ MeV. The curves show the results of four different DWBA calculations: solid, "standard set"; short dashes, with nonlocality included; long dashes, with the same real potential in both entrance and exit channels; dotted-dashed curve, with no Coulomb excitation.

resonance mixing phases $\phi^{\lambda}_{l'j'}$ could be varied. The other resonance parameters were kept fixed, since they had already been determined from the analysis of the elastic scattering excitation functions. The nonresonant scattering amplitudes and the optical-model phase shifts were calculated by HELMY at 100-keV intervals and then read by INELAS, which used linear interpolation to find the values of these quantities at each energy of interest.

In our initial attempts to fit the data, we were guided by the weak-coupling model calculations of Auerbach and Stein.[15] We included only those outgoing partial waves which corresponded to the positive-parity single-particle levels, namely, $s_{1/2}$, $d_{3/2}$, $d_{5/2}$, $g_{7/2}$, $g_{9/2}$, and $i_{11/2}$ [the $j_{15/2}$ partial wave, which could be used only with the $\frac{15}{2}^-$ IAR (level 10), was not included, since it would have been too weak to observe]. In addition, since the calculations indicated that the $|2^+\otimes i_{11/2}\rangle$ configuration contributed less than 5% to each of the parent states, and since the $i_{11/2}$ single-particle widths are small because of the large angular momentum barrier, we decided not to use the $i_{11/2}$ partial wave at all. Finally, the calculations indicated that almost all of the strength for each configuration should be concentrated within about 1.5 MeV of the unperturbed energy for that configuration; this result was used in deciding which partial waves to start with for each IAR.

We began by using just a few of the strongest IAR's, hoping to obtain a gross fit to the data. The results were encouraging: All the main features of the experimental excitation functions were reproduced, the amplitudes $\gamma^{\lambda}_{l'j'}$ were not too large (compared to the single-particle values), and the phases $\phi^{\lambda}_{l'j'}$ were not too far from zero. This last result suggested to us that we should fix all the values of $\phi^{\lambda}_{l'j'}$ at zero. This halved the number of variable parameters, making it possible for us to add more IAR's and to include more outgoing waves for each IAR. Eventually, all but one of the positive-parity IAR's were included in the fit; the one exception was the IAR of level 2 ($\frac{5}{2}^+$), for which the predominant configuration was known[23] to be

$$|(^{208}\text{Pb } 3^-)\otimes(p_{1/2})^{-1}\rangle .$$

Also, all of the allowed $l'=0$, 2, and 4 partial waves were used for each IAR, even if the IAR was more than 1.5 MeV away from the appropriate unperturbed energies.

Some problems began to appear as more IAR's were included, particularly when corresponding parameters for neighboring IAR's which had the same spin and parity were varied simultaneously. In several such cases $\gamma^{\lambda}_{l'j'}$ would become very large and positive for one of the IAR's, while becoming very large and negative for the other. To prevent this, we divided the IAR's into three classes, so that we could vary all the parameters in one class while keeping the parameters in the other two classes fixed. The fitting was then done by iteration, until all three classes could be varied, one after another, without producing more than a 5% change in χ^2_ν.

The resulting fits to the inelastic scattering excitation functions are shown in Figs. 6–9. Also shown in those figures are the cross sections and analyzing powers that we computed using only the DWBA background, with no IAR's included. The agreement between the fit and the data is excellent, with the fit reproducing essentially every feature of the experimental excitation functions.

Table IV shows the best-fit values for the inelastic partial width amplitudes $\gamma^{\lambda}_{l'j'}$ (with all of the phases fixed at $\phi^{\lambda}_{l'j'}=0$). The error shown for each amplitude comes from the last calculation in which that amplitude was varied; since the values of $\gamma^{\lambda}_{l'j'}$ were not all varied at the same time, it is not always possible to make comparisons between the quoted errors for different IAR's. The errors do not take into account the effects of uncertainties in the other (fixed) resonance parameters or in the DWBA background.

V. SINGLE-PARTICLE WIDTHS AND SPECTROSCOPIC AMPLITUDES

In order to extract spectroscopic information from the experimental partial widths and partial width amplitudes, we needed to use a theory of isobaric analog resonances. Many such theories appeared in the literature during the years immediately following the discovery of the IAR. Some of them, such as those of Thompson, Adams, and Robson (TAR)[36] and Zaidi, Darmodjo, and Harney (ZDH),[37] have been used by previous authors[12,13] for the analysis of experimental data. In the present work, the theory of Bund and Blair (BB)[38] was used. Although BB and ZDH were developed using rather different approaches, they give the same answers for the single-particle widths; these answers, however, differ by as much as 20–30% from those given by TAR. This disagreement among competing theories has long been one of the main problems with the IAR method.

A number of assumptions and approximations were used in the development of BB, the most significant being the use of a phenomenological optical-model potential for the proton channels. Since this potential had no channel-channel coupling terms, direct inelastic scattering was excluded from the theory. This simplification appears to be

TABLE IV. Partial width amplitudes $\gamma^{\lambda}_{l'j'}$ (in keV$^{1/2}$) for the decay of isobaric analog resonances in ^{207}Bi to the 2^+ (E_x=0.803 MeV) state of ^{206}Pb. The phases $\phi^{\lambda}_{l'j'}$ were all set equal to zero.

Level	J^{π}	E_{λ} (MeV)	$\gamma^{\lambda}_{l'j'}$ $l'j'=s_{1/2}$	$l'j'=d_{3/2}$	$l'j'=d_{5/2}$	$l'j'=g_{7/2}$	$l'j'=g_{9/2}$
1	$\frac{7}{2}^-$	14.471			(Not included in the fit)		
2	$\frac{5}{2}^+$	14.756			(Not included in the fit)		
3	$\frac{9}{2}^+$	14.860			0.46±0.02	0.33±0.04	0.73±0.03
4	$\frac{9}{2}^+$	15.562			1.86±0.18	−1.87±0.36	−1.33±0.20
5	$\frac{11}{2}^+$	15.642				−0.45±0.23	−0.44±0.61
6	$\frac{11}{2}^+$	15.752				1.08±0.26	−3.02±0.72
7	$\frac{5}{2}^+$	15.767	−1.98±0.19	1.54±0.32	−0.39±0.19	0.77±0.22	4.40±0.13
8	$\frac{5}{2}^+$	15.857	5.07±0.32	1.52±0.46	−1.26±0.30	−1.68±0.41	−1.46±0.16
9	$\frac{5}{2}^+$	16.132	1.37±0.56	1.79±0.97	−0.81±0.47	1.63±0.62	0.91±0.25
10	$\frac{15}{2}^-$	16.247			(Not included in the fit)		
11	$\frac{5}{2}^+$	16.451	0.98±0.19	−0.22±0.26	−0.24±0.16	−1.05±0.19	−0.13±0.09
12	$\frac{5}{2}^+$	16.521	0.08±0.12	0.44±0.18	0.80±0.11	1.33±0.11	−0.71±0.07
13	$\frac{1}{2}^+$	16.670		−1.16±0.29	2.20±0.26		
14	$\frac{5}{2}^+$	16.713	−5.77±0.70	−0.17±1.04	−1.21±0.81	2.76±0.69	−0.74±0.37
15	$\frac{5}{2}^+$	16.745	2.07±0.62	3.06±0.94	0.93±0.69	2.46±0.72	1.46±0.31
16	$\frac{1}{2}^+$	16.759		−0.56±0.13	2.38±0.16		
17	$\frac{1}{2}^+$	16.773		0.46±0.42	0.01±0.54		
18	$\frac{7}{2}^+$	17.003		−1.04±0.19	1.24±0.41	0.55±0.19	0.97±0.33
19	$\frac{1}{2}^+$	17.117		6.25±0.35	−6.35±0.28		
20	$\frac{7}{2}^+$	17.189		2.46±0.75	−6.60±0.76	2.39±0.60	−1.47±0.88
21	$\frac{3}{2}^+$	17.204	−1.34±0.84	0.18±0.67	1.70±0.68	−1.40±0.67	
22	$\frac{3}{2}^+$	17.212	1.20±0.42	0.34±0.39	0.23±0.47	0.47±0.37	
23	$\frac{3}{2}^+$	17.262	1.83±0.85	0.22±0.73	1.13±0.62	−3.07±0.50	
24	$\frac{7}{2}^+$	17.313		1.06±0.20	2.50±0.25	0.53±0.21	−1.33±0.26
25	$\frac{3}{2}^+$	17.337	1.87±0.45	2.53±0.48	0.77±0.55	1.58±0.42	
26	$\frac{3}{2}^+$	17.351	−0.83±0.22	−0.48±0.22	−2.88±0.18	1.21±0.19	
27	$\frac{7}{2}^+$	17.401		0.59±0.60	0.47±0.45	0.22±0.45	0.94±0.87
28	$\frac{7}{2}^+$	17.445		0.67±0.67	−8.15±0.61	0.13±0.63	0.32±0.88
29	$\frac{7}{2}^+$	17.502		0.88±0.38	1.57±0.43	0.81±0.36	0.87±0.45
30	$\frac{7}{2}^+$	17.564		−1.79±1.00	1.17±1.23	2.74±0.57	0.30±1.08
31	$\frac{3}{2}^+$	17.625	0.95±0.50	0.42±0.54	0.81±0.98	2.33±0.55	
32	$\frac{3}{2}^+$	17.635	−5.62±0.35	2.31±0.39	2.33±0.55	−3.91±0.41	
33	$\frac{3}{2}^+$	17.707	−4.63±1.08	4.90±0.80	−1.14±2.32	−2.09±1.24	
34	$\frac{7}{2}^+$	17.750		−0.79±1.51	−3.64±1.51	0.06±1.09	0.40±1.94
35	$\frac{3}{2}^+$	17.824	−0.54±1.52	3.11±1.60	6.30±3.68	3.63±1.54	

justified in the present case, since the cross sections for direct inelastic scattering are small compared to the elastic scattering cross sections. Nevertheless, it does seem to introduce an inconsistency, since for the 2^+ state of ^{206}Pb the direct and resonance contributions to the inelastic scattering are comparable in magnitude.

Bund and Blair were able to obtain explicit expressions for all of the resonance parameters for an isolated IAR. In particular, they found that the partial widths and the "intrinsic phases" were given by

$$[\Gamma_p^{\nu,lj}\exp(i\phi_{\nu,lj})]^{1/2}=\left[\frac{4\mu}{\hbar^2 k_\nu}\right]^{1/2}(2T_0+1)^{-1/2}\theta_{\nu,lj}\int_0^\infty W_{\nu,lj}(r)V_1(r)Q_{lj}(r,E_\nu)dr\ . \tag{7}$$

In this expression, each channel is characterized by an index ν, which denotes the state of the residual nucleus ($\nu=0$ being the ground state), and by the angular momentum quantum numbers l and j of the proton. The index λ which identifies the IAR has been suppressed. Note that, because of differences in definitions, the partial widths and the phases given in BB are not quite the same as those used elsewhere in this paper; instead, these quantities are related by

$$\Gamma_{lj}^{\lambda}=\Gamma_{\mathrm{p}}^{0,lj},\quad \Gamma_{l'j'}^{\lambda}=(k_0/k_\nu)\Gamma_{\mathrm{p}}^{\nu,l'j'},$$
$$\phi_{lj}^{\lambda}+\delta_{lj}=\tfrac{1}{2}\phi_{0,lj},\quad \phi_{l'j'}^{\lambda}+\delta_{l'j'}'=\tfrac{1}{2}\phi_{\nu,l'j'}.$$

The radial wave function $Q_{lj}(r,E_\nu)$ which appears in Eq. (7) is the regular solution of the Schrödinger equation for an unbound proton of energy E_ν in the complex potential $V_{\mathrm{p}}(r)$; it is normalized to a linear combination of incoming and outgoing Coulomb waves in the asymptotic region. The other radial wave function, $W_{\nu,lj}(r)$, is the normalized eigenfunction for a bound neutron in the real potential $V_{\mathrm{n}}(r)$. The third factor in the integrand is the isospin potential

$$V_1(r)\equiv V_{\mathrm{n}}(r)-V_{\mathrm{p}}(r)+V_C(r);$$

it consists of both the symmetry potential and the proton imaginary potential [but not the Coulomb potential $V_C(r)$]. In the present work, the optical-model potential which gave the best fit to the elastic scattering angular distributions (set B of Table III) was used for $V_{\mathrm{p}}(r)$. The neutron potential $V_{\mathrm{n}}(r)$ was then required to have the same spin-orbit potential and the same real geometry as $V_{\mathrm{p}}(r)$; however, it had a different value for the depth of the real potential. This depth was adjusted so that the eigenfunction $W_{\nu,lj}(r)$ would have a binding energy equal to the experimental neutron separation energy (corrected by subtracting the excitation energy of the parent state and adding that of the residual nucleus).

Also appearing in Eq. (7) are the target isospin T_0 and the spectroscopic amplitude $\theta_{\nu,lj}$, which is just the coefficient of fractional parentage between the parent state and the particle-core configuration $|\nu\otimes lj\rangle$ [cf. Eq. (1)]. The square of this quantity is the spectroscopic factor $S_{\nu,lj}$. Note that if we set $\theta_{\nu,lj}$ equal to 1 and then use Eq. (7) to calculate the partial width, what we get is the single-particle width $\Gamma_{\mathrm{sp}}^{\nu,lj}$. The actual spectroscopic amplitude can then be determined from

$$(\Gamma_{\mathrm{p}}^{\nu,lj})^{1/2}=\theta_{\nu,lj}(\Gamma_{\mathrm{sp}}^{\nu,lj})^{1/2}$$

by using the experimental partial width amplitude on the left-hand side.

The calculations outlined above were performed using Bund's program ANALOG.[38] We made some modifications to this program, the most significant being the introduction of nonlocality. The proton and neutron wave functions were computed using local potentials and were then damped as prescribed by Perey[34] using the standard[35] nonlocality length (0.85 fm). The damped neutron wave function then had to be renormalized; the net effect for the neutron was thus to enhance its wave function in the tail region (where the potential was small) and to reduce it in the interior (where the potential was large). Since the largest contribution to the integral in Eq. (7) was from the nuclear interior, the nonlocality correction caused all of the single-particle widths to become smaller.

The procedures described here were tested using the single-particle IAR's in ^{209}Bi, since the spectroscopic factors for the parent states (with the possible exception of the $j_{15/2}$ state[39]) were expected to be near unity. What we found[18] was that all of the spectroscopic factors were between 0.90 and 1.06 (except for the $i_{11/2}$ state, for which $S_{0,lj}=0.78\pm0.08$). We also computed the values of the single-particle widths as functions of energy; the results are shown in Fig. 11. These may be compared with the results of similar calculations for IAR's in ^{208}Bi, which were done using both ZDH and TAR.[12] The ZDH single-particle widths were about 40–50 % higher than ours, apparently because nonlocality corrections had not been made. To check this, we did some sample ANALOG calculations for ^{209}Bi, in which we did not use nonlocality; those results were then in good agreement with the ^{208}Bi ZDH results.

The ANALOG calculations for the IAR's in ^{207}Bi gave results which were almost identical to those shown in Fig. 11, except that the single-particle widths were about 1–4 % higher for $l=0$, 2, and 4, and about 1–5 % lower for $l=6$ and 7. For each value of j, the ratio of the ^{207}Bi and ^{209}Bi single-particle widths was a constant (to within $\pm0.4\%$) over the entire energy range. This shows that we were justified in using the ^{209}Bi single-particle widths to fix the ratios of the elastic partial widths in Sec. III.

The single-particle spectroscopic factors $S_{0,lj}$ for all 35 parent states in ^{207}Pb are shown in Table V. The error bars are given only for the strongest state in each group, and they reflect only the errors in the experimental partial

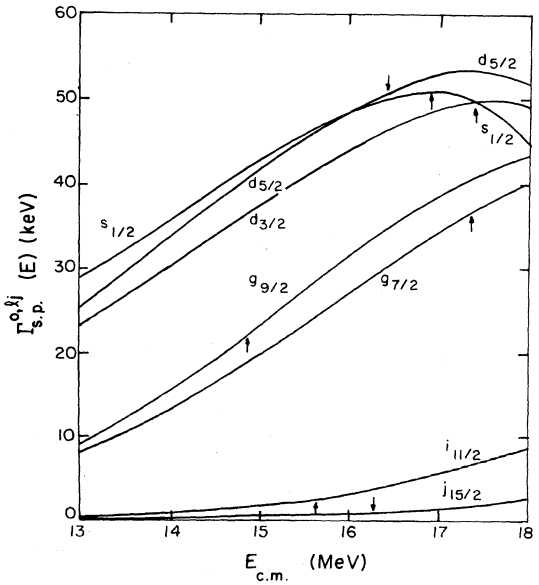

FIG. 11. Single-particle widths for IAR's in ^{209}Bi, shown as functions of proton energy. The arrows indicate the locations of the actual IAR's.

TABLE V. Results of ANALOG calculations for the isobaric analog resonances of states in ^{207}Pb. The values of E_λ and Γ^λ_{lj} are taken from Table II, while the values of ϕ^λ_{lj} and $\Gamma^{0,lj}_{sp}$ are given by the calculations. The ratio of Γ^λ_{lj} to $\Gamma^{0,lj}_{sp}$ for each state is the spectroscopic factor $S_{0,lj}$ for that state.

Level	nlj	E_λ (MeV)	ϕ^λ_{lj} (deg)	$\Gamma^{0,lj}_{sp}$ (keV)	Γ^λ_{lj} (keV)	$S_{0,lj}$
1	$2f_{7/2}$	14.471	31.3	33.37	0.52	0.016
2	$3d_{5/2}$	14.756	13.0	42.19	0.15	0.004
3	$2g_{9/2}$	14.860	8.8	22.46	19.44±0.27	0.866±0.012
4	$2g_{9/2}$	15.562	9.3	28.62	0.66	0.023
5	$1i_{11/2}$	15.642	4.9	2.45	1.25±0.08	0.510±0.033
6	$1i_{11/2}$	15.752	5.0	2.62	1.10	0.420
7	$3d_{5/2}$	15.767	11.4	49.43	4.17±0.21	0.084±0.004
8	$3d_{5/2}$	15.857	11.2	49.99	0.81	0.016
9	$3d_{5/2}$	16.132	10.7	51.59	0.68	0.013
10	$1j_{15/2}$	16.247	2.8	0.78	1.03±0.14	1.321±0.179
11	$3d_{5/2}$	16.451	10.0	53.21	6.70	0.126
12	$3d_{5/2}$	16.521	9.8	53.53	27.32±0.59	0.510±0.011
13	$4s_{1/2}$	16.670	10.5	52.39	3.72	0.071
14	$3d_{5/2}$	16.713	9.4	54.32	0.83	0.015
15	$3d_{5/2}$	16.745	9.3	54.44	0.62	0.011
16	$4s_{1/2}$	16.759	10.2	52.51	47.79±1.40	0.910±0.027
17	$4s_{1/2}$	16.773	10.1	52.53	3.37	0.064
18	$2g_{7/2}$	17.003	10.9	35.51	1.84±0.20	0.052±0.006
19	$4s_{1/2}$	17.117	8.7	52.55	4.16	0.079
20	$2g_{7/2}$	17.189	10.8	36.80	1.48	0.040
21	$3d_{3/2}$	17.204	10.2	51.07	1.40	0.027
22	$3d_{3/2}$	17.212	10.2	51.09	1.82	0.036
23	$3d_{3/2}$	17.262	10.0	51.20	5.55	0.108
24	$2g_{7/2}$	17.313	10.7	37.64	14.29±0.68	0.380±0.018
25	$3d_{3/2}$	17.337	9.8	51.34	4.28	0.083
26	$3d_{3/2}$	17.351	9.7	51.37	32.40±0.76	0.631±0.015
27	$2g_{7/2}$	17.401	10.6	38.23	1.05	0.027
28	$2g_{7/2}$	17.445	10.5	38.52	4.62±0.34	0.120±0.009
29	$2g_{7/2}$	17.502	10.5	38.88	1.33	0.034
30	$2g_{7/2}$	17.564	10.4	39.28	3.69	0.094
31	$3d_{3/2}$	17.625	8.8	51.64	1.04	0.020
32	$3d_{3/2}$	17.635	8.8	51.64	1.90	0.037
33	$3d_{3/2}$	17.707	8.6	51.64	2.33	0.045
34	$2g_{7/2}$	17.750	10.2	40.42	1.11	0.027
35	$3d_{3/2}$	17.824	8.1	51.56	0.92	0.018

widths; no uncertainties have been assigned to the calculated single-particle widths. In Table VI we show the spectroscopic amplitudes $\theta_{2^+,l'j'}$ for 32 of the parent states, using the same format that we used for the experimental partial width amplitudes (Table IV). Note that each spectroscopic amplitude has the same sign as the corresponding partial width amplitude, since the square root of the single-particle width was always positive.

VI. DISCUSSION

A. Sum rules

The spectroscopic amplitudes $\theta_{\nu,lj}$ are subject to certain constraints because of orthonormality and completeness requirements. Since we are dealing with a truncated set of states λ and configurations $|\nu\otimes lj\rangle$, these constraints take the form of inequalities. One of them comes from the normalization requirement for the individual states,

$$N_\lambda \equiv \sum_{\nu,j} (\theta^\lambda_{\nu,lj})^2 \leq 1 \ . \tag{8}$$

The sum here is over all the single-particle states (lj) and target states (ν) that contribute to the state λ (the superscript has been added to $\theta_{\nu,lj}$ to avoid confusion). Another inequality is derived from the completeness requirement,

$$C^J_{\nu,lj} \equiv \sum_\lambda (\theta^\lambda_{\nu,lj})^2 \leq 1 \ . \tag{9}$$

Here the sum is over all states having the same J^π. Thus N_λ tells us how much of each state is accounted for in our restricted basis, while $C^J_{\nu,lj}$ tells us how much of each particle-core configuration is present in the set of states we

TABLE VI. Spectroscopic amplitudes $\theta_{2^+,l'j'}$ for the $|(2_1^+ \otimes l'j')_{J^\pi}$ components of states in ^{207}Pb.

Level	J^π	E_λ (MeV)	$\theta_{2^+,l'j'}$ $l'j'=s_{1/2}$	$l'j'=d_{3/2}$	$l'j'=d_{5/2}$	$l'j'=g_{7/2}$	$l'j'=g_{9/2}$
3	$\frac{9}{2}^+$	14.860			0.075±0.004	0.086±0.009	0.180±0.008
4	$\frac{9}{2}^+$	15.562			0.282±0.027	−0.425±0.083	−0.282±0.042
5	$\frac{11}{2}^+$	15.642				0.100±0.051	−0.091±0.129
6	$\frac{11}{2}^+$	15.752				0.236±0.058	−0.620±0.148
7	$\frac{5}{2}^+$	15.767	−0.289±0.028	0.240±0.050	−0.059±0.028	0.169±0.048	0.902±0.026
8	$\frac{5}{2}^+$	15.857	0.737±0.046	0.235±0.071	−0.187±0.045	−0.362±0.088	−0.295±0.033
9	$\frac{5}{2}^+$	16.132	0.197±0.080	0.272±0.147	0.117±0.068	0.336±0.128	0.174±0.048
11	$\frac{5}{2}^+$	16.451	0.138±0.027	−0.032±0.038	−0.034±0.022	−0.205±0.037	−0.023±0.016
12	$\frac{5}{2}^+$	16.521	0.011±0.017	0.065±0.026	0.113±0.016	0.259±0.021	−0.128±0.012
13	$\frac{1}{2}^+$	16.670		−0.170±0.043	0.308±0.036		
14	$\frac{5}{2}^+$	16.713	−0.804±0.098	−0.024±0.151	−0.168±0.113	0.521±0.131	−0.130±0.066
15	$\frac{5}{2}^+$	16.745	0.289±0.087	0.446±0.136	0.130±0.096	0.463±0.135	0.256±0.054
16	$\frac{1}{2}^+$	16.759		−0.082±0.019	0.330±0.023		
17	$\frac{1}{2}^+$	16.773		0.067±0.061	0.001±0.075		
18	$\frac{7}{2}^+$	17.003		−0.150±0.027	0.170±0.056	0.101±0.035	0.165±0.055
19	$\frac{1}{2}^+$	17.117		0.893±0.050	−0.867±0.038		
20	$\frac{7}{2}^+$	17.189		0.350±0.106	−0.898±0.104	0.424±0.106	−0.245±0.146
21	$\frac{3}{2}^+$	17.204	−0.183±0.115	0.026±0.095	0.231±0.092	−0.249±0.118	
22	$\frac{3}{2}^+$	17.212	0.165±0.058	0.049±0.055	0.031±0.063	0.084±0.066	
23	$\frac{3}{2}^+$	17.262	0.250±0.117	0.032±0.104	0.154±0.084	−0.540±0.088	
24	$\frac{7}{2}^+$	17.313		0.150±0.029	0.338±0.034	0.093±0.037	−0.218±0.042
25	$\frac{3}{2}^+$	17.337	0.256±0.061	0.357±0.068	0.104±0.074	0.275±0.074	
26	$\frac{3}{2}^+$	17.351	−0.113±0.030	−0.067±0.031	−0.389±0.024	0.212±0.033	
27	$\frac{7}{2}^+$	17.401		0.083±0.085	0.064±0.061	0.038±0.077	0.152±0.141

TABLE VI. (*Continued.*)

Level	J^π	E_λ (MeV)	$\theta_{\lambda^+,l'j'}$ $l'j'=s_{1/2}$	$l'j'=d_{3/2}$	$l'j'=d_{5/2}$	$l'j'=g_{7/2}$	$l'j'=g_{9/2}$
28	$\frac{7}{2}^+$	17.445		0.095±0.095	−1.098±0.083	0.022±0.109	0.051±0.142
29	$\frac{7}{2}^+$	17.502		0.123±0.053	0.211±0.058	0.139±0.062	0.140±0.073
30	$\frac{7}{2}^+$	17.564		−0.250±0.140	0.157±0.166	0.467±0.096	0.048±0.173
31	$\frac{3}{2}^+$	17.625	0.129±0.069	0.058±0.076	0.108±0.132	0.394±0.093	
32	$\frac{3}{2}^+$	17.635	−0.767±0.048	0.323±0.054	0.312±0.074	−0.660±0.069	
33	$\frac{3}{2}^+$	17.707	−0.632±0.148	0.683±0.111	−0.152±0.310	−0.351±0.208	
34	$\frac{7}{2}^+$	17.750		−0.109±0.210	−0.486±0.201	0.010±0.182	0.063±0.306
35	$\frac{3}{2}^+$	17.824	−0.074±0.207	0.432±0.222	0.839±0.490	0.602±0.255	

TABLE VII. The spectroscopic sum $N_\lambda \equiv \sum_{\nu,j}(\theta^\lambda_{\nu,lj})^2$ for each state (λ) in ^{207}Pb. For levels 1, 2, and 10, the sum includes only $(\theta^\lambda_{0,lj})^2$.

Level	J^π	E_λ (MeV)	N_λ
1	$\frac{7}{2}^-$	14.471	0.016
2	$\frac{5}{2}^+$	14.756	0.004±0.000
3	$\frac{9}{2}^+$	14.860	0.911±0.013
4	$\frac{9}{2}^+$	15.562	0.363±0.076
5	$\frac{11}{2}^+$	15.642	0.528±0.042
6	$\frac{11}{2}^+$	15.752	0.861±0.187
7	$\frac{5}{2}^+$	15.767	1.071±0.058
8	$\frac{5}{2}^+$	15.857	0.868±0.102
9	$\frac{5}{2}^+$	16.132	0.283±0.124
10	$\frac{15}{2}^-$	16.247	1.321±0.179
11	$\frac{5}{2}^+$	16.451	0.190±0.017
12	$\frac{5}{2}^+$	16.521	0.610±0.017
13	$\frac{1}{2}^+$	16.670	0.195±0.027
14	$\frac{5}{2}^+$	16.713	0.979±0.212
15	$\frac{5}{2}^+$	16.745	0.590±0.034
16	$\frac{1}{2}^+$	16.759	1.026±0.031
17	$\frac{1}{2}^+$	16.773	0.068±0.008
18	$\frac{7}{2}^+$	17.003	0.140±0.029
19	$\frac{1}{2}^+$	17.117	1.628±0.111
20	$\frac{7}{2}^+$	17.189	1.210±0.231
21	$\frac{3}{2}^+$	17.204	0.178±0.084
22	$\frac{3}{2}^+$	17.212	0.073±0.023
23	$\frac{3}{2}^+$	17.262	0.488±0.115
24	$\frac{7}{2}^+$	17.313	0.572±0.036
25	$\frac{3}{2}^+$	17.337	0.362±0.073
26	$\frac{3}{2}^+$	17.351	0.845±0.028
27	$\frac{7}{2}^+$	17.401	0.062±0.046
28	$\frac{7}{2}^+$	17.445	1.338±0.184
29	$\frac{7}{2}^+$	17.502	0.133±0.038
30	$\frac{7}{2}^+$	17.564	0.402±0.127
31	$\frac{3}{2}^+$	17.625	0.207±0.081
32	$\frac{3}{2}^+$	17.635	1.262±0.131
33	$\frac{3}{2}^+$	17.707	1.056±0.297
34	$\frac{7}{2}^+$	17.750	0.279±0.204
35	$\frac{3}{2}^+$	17.824	1.277±0.900

are considering.

From Table VII we see that the spectroscopic sums N_λ are less than 1.0 (within the error bars) for all but five of the ^{207}Pb states that we have studied. Of those five, only level 19 has a value of N_λ which exceeds 1.0 by more than

TABLE VIII. The spectroscopic sum $C^J_{\nu,lj} \equiv \sum_\lambda (\theta^\lambda_{\nu,lj})^2$ for each of the configurations $|(\nu \otimes lj)_{J^\pi}\rangle$ in ^{207}Pb. For $\nu = 2^+$, the weighted average sums $C_{2^+,lj}$ are given in the bottom row.

J^π	$C^J_{0,lj}$	$lj = s_{1/2}$	$lj = d_{3/2}$	$C^J_{2^+,lj}$ $lj = d_{5/2}$	$lj = g_{7/2}$	$lj = g_{9/2}$
$\frac{9}{2}^+$	0.889±0.012			0.085±0.015	0.188±0.070	0.112±0.024
$\frac{11}{2}^+$	0.930±0.060				0.066±0.029	0.393±0.185
$\frac{5}{2}^+$	0.779±0.015	1.415±0.182	0.392±0.152	0.111±0.051	0.868±0.215	1.030±0.063
$\frac{1}{2}^+$	1.124±0.033		0.838±0.091	0.955±0.071		
$\frac{7}{2}^+$	0.774±0.030		0.273±0.116	2.465±0.332	0.438±0.129	0.186±0.100
$\frac{3}{2}^+$	1.005±0.024	1.211±0.219	0.896±0.253	1.077±0.950	1.559±0.379	
		1.333±0.140	0.490±0.083	0.915±0.155	0.441±0.059	0.375±0.067

two error bars. The agreement with inequality (8), then, appears to be very good. Note that for many states N_λ is quite small. This means that we would need to use a larger basis in order to obtain a complete description of those states. For example, some of them could have large spectroscopic amplitudes for the $|2_2^+ \otimes lj\rangle$ or $|4_1^+ \otimes lj\rangle$ configurations, in addition to the amplitudes given here.

The information in Tables V and VII is displayed graphically in Fig. 12. In that figure, each of the positive-parity states is represented by a vertical bar of height N_λ; the heights of the shaded and blank portions give the values of $S^\lambda_{0,lj}$ and $\sum_{j'}(\theta^\lambda_{2^+,l'j'})^2$, respectively. The dashed line at $N_\lambda = 1$ indicates the upper limit given by inequality (8).

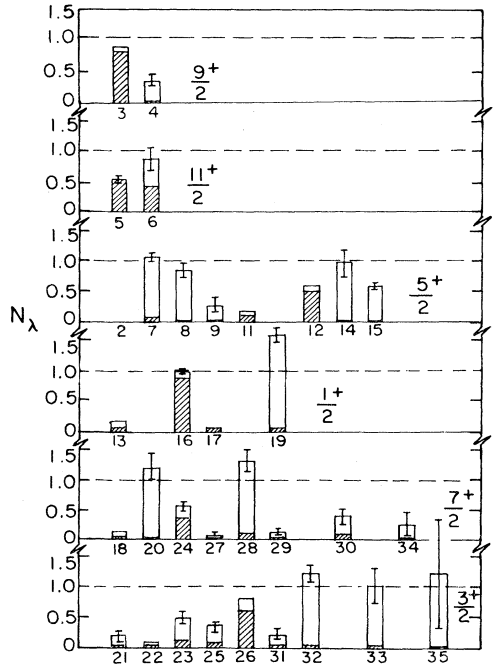

FIG. 12. Spectroscopic sums (N_λ) for some positive-parity states in ^{207}Pb. The states are grouped according to their J^π and are identified by their level numbers. The shaded portion of each vertical bar indicates the value of $S^\lambda_{0,lj}$; the open portion indicates the value of $\sum_{j'}(\theta^\lambda_{2^+,l'j'})^2$. The error bar is not shown if $\delta N_\lambda < 0.03$.

We see from Table VIII that inequality (9) is satisfied for all but one of the single-particle configurations. For $s_{1/2}$, the value of $C^J_{0,lj}$ is 12% too high; however, this is consistent with the results for ^{209}Pb,[18] where the $s_{1/2}$ single-particle strength was found to be 6% too high. It is interesting to note that, even with the large number of $\frac{5}{2}^+$ and $\frac{7}{2}^+$ IAR's that we observed in the ^{206}Pb elastic scattering, we are still missing 22% of the single-particle strength for each of those configurations.

We also see from Table VIII that only three of the values of $C^J_{2^+,lj}$ exceed 1.0 by more than one error bar; one of those three, however, is very large. At this point, it is instructive to consider the weighted average strength for each particle-core configuration,[13]

$$C_{\nu,lj} \equiv \frac{\sum_J (2J+1) C^J_{\nu,lj}}{\sum_J (2J+1)} ,$$

which tells us the fraction of the total strength for each configuration that is present in the states we observed, irrespective of angular-momentum coupling. The values of $C_{\nu,lj}$ are displayed in Fig. 13 for both $\nu = 0^+$ and 2^+; they are also given (for $\nu = 2^+$) in the bottom row of Table VIII. It appears that the value of $C_{2^+,lj}$ is too large for $lj = s_{1/2}$ and that it is too small for some of the other lj's. For the $|2^+ \otimes d_{3/2}\rangle$ and $|2^+ \otimes g_{7/2}\rangle$ configurations, however, the low total strength is not surprising, since the unperturbed energy for each of these configurations is higher than the energies of the states we observed. It should also be remembered that the $|2^+ \otimes i_{11/2}\rangle$ configuration was neglected in this analysis. Our results might have been slightly different if that configuration had been included.

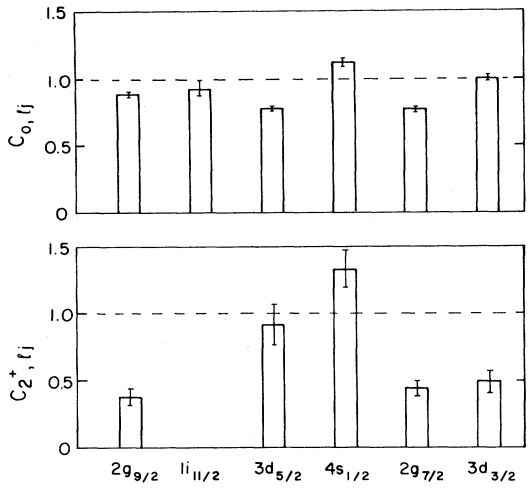

FIG. 13. Spectroscopic sums ($C_{v,lj}$) for the $|0^+\otimes lj\rangle$ and $|2^+\otimes lj\rangle$ configurations in ^{207}Pb.

B. Comparison to previous work

Although the IAR's in ^{207}Bi have been studied by a number of authors,[2,4,7,11] most of the studies have concentrated on the lower-energy resonances, such as the IAR's of the ground state and the strong $\frac{9}{2}^+$ state of ^{207}Pb. There have been no systematic elastic scattering studies covering a broad energy range. However, there has been a study of the inelastic scattering to the first 2^+ state of ^{206}Pb between $E_p=14.2$ and 17.3 MeV by Ayoub, Ascuitto, and Bromley[26] (using unpolarized protons). They measured several angular distributions between $E_p=15.80$ and 16.90 MeV, and they were able to fit them by using ten IAR's and varying only the phases ($\phi^\lambda_{lj}+\phi^\lambda_{l'j'}$). They fixed the values of E_λ for these resonances by making the energy of the strong $\frac{9}{2}^+$ IAR the same as the energy of the $\frac{9}{2}^+$ IAR in ^{209}Bi,[8] and then requiring the other resonance energies to be consistent with the ^{206}Pb(d,p) results of Moyer, Cohen, and Diehl.[21] Also, they used the values of Γ_λ that had been found by Wharton *et al.*[8] for ^{209}Bi. Finally, they computed the partial widths for the elastic and 2^+ channels by multiplying the partial widths for the corresponding IAR's in ^{209}Bi (Ref. 8) by the weak-coupling model spectroscopic factors calculated by Auerbach and Stein.[15] The fits to their angular distributions were generally good. Unfortunately, it is difficult to compare their work with ours, not only because we used more IAR's, but also because their basic approach was quite different from ours. We wanted to find the best values of the elastic and inelastic resonance parameters by varying them to fit the data. Their purpose, on the other hand, was to show that it was possible to obtain a reasonable fit to the inelastic scattering data by using reasonable resonance parameters, with a minimum of parameter variation; they also wanted to demonstrate the importance of resonance-background interference.

Our single-particle spectroscopic factors can, however, be compared directly with those found using the ^{206}Pb(d,p)^{207}Pb reaction. This reaction has been studied by Hering, Achterath, and Dost[40] in the Coulomb-stripping region (7.6–9.5 MeV), by Darcey, Jeans, and Jones[41] at 8 and 18.7 MeV, and (most recently) by Moyer, Cohen, and

TABLE IX. Spin assignments and spectroscopic factors for selected states in ^{207}Pb, deduced from (d,p) studies at various bombarding energies and from the present work.

Level	E_x[a] (MeV)	8 MeV[b] J^π	8 MeV[b] S	7.6–9.5 MeV[c] J^π	7.6–9.5 MeV[c] S	17 MeV[a] J^π	17 MeV[a] S	Present work J^π	Present work S
3	2.728	$\frac{9}{2}^+$	0.93	$\frac{9}{2}^+$	1.16	$\frac{9}{2}^+$	0.97	$\frac{9}{2}^+$	0.87±0.01
5	3.510					$\frac{11}{2}^+$	0.48	$\frac{11}{2}^+$	0.51±0.03
7	3.635	$\frac{5}{2}^+$	0.12	$\frac{5}{2}^+$	0.13	$\frac{5}{2}^+$	0.14	$\frac{5}{2}^+$	0.084±0.004
10	4.115					$\frac{15}{2}^-$	1.45	$\frac{15}{2}^-$	1.32±0.18
11	4.319	$\frac{5}{2}^+$	0.17	$\frac{5}{2}^+$	0.17	$\frac{5}{2}^+$	0.19	$\frac{5}{2}^+$	0.13
12	4.389	$\frac{5}{2}^+$	0.53	$\frac{5}{2}^+$	0.61	$\frac{5}{2}^+$	0.77	$\frac{5}{2}^+$	0.51±0.01
16	4.627	$\frac{1}{2}^+$	0.76	$\frac{1}{2}^+$	0.84	$\frac{1}{2}^+$	1.09	$\frac{1}{2}^+$	0.91±0.03
18	4.871					$\frac{7}{2}^{+d}$	0.084	$\frac{7}{2}^+$	0.052±0.006
23	5.130			$\frac{7}{2}^+$	0.86	$\frac{7}{2}^+(\frac{3}{2}^+)^e$	0.18(0.091)	$\frac{3}{2}^+$	0.11
24	5.181	$\frac{7}{2}^+$	1.00	$\frac{3}{2}^+$	0.20	$\frac{3}{2}^+(\frac{7}{2}^+)^e$	0.25(0.53)	$\frac{7}{2}^+$	0.38±0.02
26	5.219	$\frac{3}{2}^+$	0.54	$\frac{3}{2}^+$	0.67	$\frac{3}{2}^+$	0.53	$\frac{3}{2}^+$	0.63±0.02
28	5.313					$\frac{7}{2}^{+d}$	0.14	$\frac{7}{2}^+$	0.12±0.01

[a]Reference 21.
[b]Reference 41.
[c]Reference 40.
[d]The spin assignment was uncertain.
[e]The first spin assignment is the one that was preferred by the authors.

Diehl[21] at 17 MeV. Since the results of this last work have already been used to fix ratios of spectroscopic factors, it would not be very meaningful to make comparisons for all of the states that we studied. Table IX, therefore, includes only the strongest state from each group of states whose Γ_{lj}^{λ}'s were linked together, plus some additional states that were reported in Refs. 40 and/or 41. The differences in the spin assignments for these and other states have already been discussed. For the spectroscopic factors, there is fair agreement; the values given by Moyer, Cohen, and Diehl are about 20% larger than ours, except for the $d_{3/2}$ states, where they are about 20% smaller.

Finally, we attempted to compare our results with the weak-coupling model predictions of Auerbach and Stein.[15] These authors calculated the wave functions for the states in ^{207}Pb using a basis which consisted only of the $|0^+\otimes lj\rangle$ and $|(2^+\otimes l'j')_j\rangle$ configurations. The answers that they got for the energies, spins, and spectroscopic factors of these states bear only a superficial resemblance to our experimental results. There are many important features of the actual ^{207}Pb level structure, such as the $\frac{5}{2}^+$ doublet at $E_x=4.319$ and 4.389 MeV, that were not predicted by the theory. Where quantitative comparisons of the spectroscopic factors can be made, the theoretical predictions are often quite different from what we observed. For example, the predicted $g_{9/2}$ state at $E_x=3.61$ MeV can probably be identified with our level 4 at $E_x=3.430$ MeV; for this state, the predicted spectroscopic factor for the $|2^+\otimes g_{9/2}\rangle$ configuration is 0.93, while the corresponding experimental value is only 0.08 ± 0.02. On the other hand, the predicted spectroscopic factors for the strong $s_{1/2}$ state (level 16) are 0.21 (versus 0.11 ± 0.02 observed) for $|2^+\otimes d_{5/2}\rangle$ and 0.02 (versus 0.007 ± 0.003) for $|2^+\otimes d_{3/2}\rangle$, so there is reasonably good agreement for that state.

These comparisons demonstrate the need for better theoretical calculations, using bases which contain configurations built on additional excited states of ^{206}Pb (2_2^+, 4_1^+, 2_3^+, etc.). A step in that direction has already been taken by Mukherjee, Chalapati Rao, and Mukherjee.[42] They considered the coupling between configurations built not only on the ground state and the "one-phonon" state (2^+, $E_x=0.803$ MeV) of ^{206}Pb, but also on the "two-phonon" states. This additional coupling produced a more complicated level scheme for ^{207}Pb, with greater fragmentation of the single-particle strengths, especially for $d_{5/2}$ and $d_{3/2}$. For the lower-lying states, there was some marginal improvement in the agreement with our experimental spectroscopic factors, particularly for the $\frac{5}{2}^+$ doublet mentioned above. For the higher-lying states, however, their energies and spectroscopic factors were still very different from ours. Thus, until even more sophisticated model calculations are performed, it will not be possible to make detailed comparisons between our results and the predictions of the weak-coupling model.

VII. CONCLUSIONS

This work demonstrates again the utility of the isobaric analog resonance method for obtaining spectroscopic information. By analyzing our elastic scattering data, we found spectroscopic factors for states in ^{207}Pb that were comparable in magnitude (and accuracy) to those found using stripping reactions. Also, since we measured both the cross sections and the analyzing powers, we were able to obtain a consistent set of spin-parity assignments. Finally, the analysis of our inelastic scattering data gave us information on the $|2^+\otimes lj\rangle$ components of the ^{207}Pb wave functions which could not be obtained in any other way. We hope that this work will stimulate new theoretical calculations for the ^{207}Pb level structure, since the existing weak-coupling model predictions are clearly inadequate to describe our experimental results.

ACKNOWLEDGMENTS

We wish to thank Professor Thomas A. Trainor, Dr. Richard von Lintig, and Dr. Hyoung Bhang, who assisted in the design of the experiment and in the gathering of the data. We are also grateful to the late Professor John S. Blair for his insights and thought-provoking questions during the analysis phase. This work was supported in part by the U.S. Department of Energy.

*Present address: Lawrence Livermore National Laboratory, Livermore, CA 94550.

†Present address: Hahn-Meitner-Institut für Kernforschung, D-1000 Berlin 39, Federal Republic of Germany.

[1]J. D. Fox, C. F. Moore, and D. Robson, Phys. Rev. Lett. 12, 198 (1964).

[2]C. D. Kavaloski, J. S. Lilley, Patrick Richard, and Nelson Stein, Phys. Rev. Lett. 16, 807 (1966).

[3]B. L. Andersen, J. P. Bondorf, and B. S. Madsen, Phys. Lett. 22, 651 (1966).

[4]G. H. Lenz and G. M. Temmer, Phys. Lett. 24B, 368 (1967); Nucl. Phys. A112, 625 (1968).

[5]S. A. A. Zaidi, J. L. Parish, J. G. Kulleck, C. Fred Moore, and P. von Brentano, Phys. Rev. 165, 1312 (1968).

[6]C. Fred Moore, J. G. Kulleck, Peter von Brentano, and Frank Rickey, Phys. Rev. 164, 1559 (1967).

[7]Nelson Stein, C. A. Whitten, Jr., and D. A. Bromley, Phys. Rev. Lett. 20, 113 (1968).

[8]W. R. Wharton, P. von Brentano, W. K. Dawson, and Patrick Richard, Phys. Rev. 176, 1424 (1968).

[9]J. L. Adams, W. J. Thompson, and D. Robson, Nucl. Phys. 89, 377 (1966).

[10]M. P. Baker, J. S. Blair, J. G. Cramer, E. Preikschat, and W. Weitkamp, in *Proceedings of the Fourth International Symposium on Polarization Phenomena in Nuclear Physics*, edited by W. Grüebler and V. König (Birkhäuser, Basel, 1976), p. 781.

[11]N. L. Back, M. P. Baker, J. G. Cramer, and T. A. Trainor, Phys. Rev. C 17, 2053 (1978).

[12]G. Latzel and H. Paetz gen. Schieck, Nucl. Phys. A323, 413 (1979).

[13]H. Clement, G. Graw, R. Zenger, and G. Zöllner, Nucl. Phys. A285, 109 (1977).
[14]A. de-Shalit, Phys. Rev. 122, 1530 (1961).
[15]N. Auerbach and N. Stein, Phys. Lett. 27B, 122 (1968).
[16]Target material was supplied by Oak Ridge National Laboratory.
[17]E. G. Adelberger, W. B. Ingalls, H. E. Swanson, and T. A. Trainor, Nuclear Physics Laboratory Annual Report, University of Washington, 1977, p. 157.
[18]N. L. Back, Ph.D. thesis, University of Washington, 1982.
[19]M. A. Melkanoff, T. Sawada, and J. Raynal, in *Methods in Computational Physics,* edited by B. Alder, S. Fernbach, and M. Rotenberg (Academic, New York, 1966), Vol. 6, p. 1.
[20]This linking feature was also used in the other programs mentioned in this paper, as was the fitting procedure described for IAR4.
[21]R. A. Moyer, B. L. Cohen, and R. C. Diehl, Phys. Rev. C 2, 1898 (1970).
[22]G. A. Bartholomew, I. Bergqvist, E. D. Earle, and A. J. Ferguson, Can. J. Phys. 48, 687 (1970).
[23]W. T. Wagner, G. M. Crawley, and G. R. Hammerstein, Phys. Rev. C 11, 486 (1975).
[24]C. P. Swann, J. Franklin Inst. 298, 321 (1974).
[25]T. Chapuran, R. Vodhanel, and M. K. Brussel, Phys. Rev. C 22, 1420 (1980).
[26]E. E. Ayoub, R. J. Ascuitto, and D. A. Bromley, Phys. Rev. Lett. 29, 182 (1972).
[27]F. D. Becchetti, Jr., and G. W. Greenlees, Phys. Rev. 182, 1190 (1969).
[28]L. R. B. Elton, *Nuclear Sizes* (Oxford University Press, London, 1961), p. 36.
[29]T. Mo and R. H. Davis, Phys. Rev. C 6, 231 (1972).
[30]J. S. Eck and W. J. Thompson, Nucl. Phys. A237, 83 (1975).
[31]H. Sherif, Ph.D. thesis, University of Washington, 1968.
[32]G. R. Satchler, *Lectures in Theoretical Physics* (Gordon and Breach, New York, 1966), Vol. VIII C, p. 95.
[33]G. Vallois, J. Saudinos, and O. Beer, Phys. Lett. 24B, 512 (1967).
[34]F. G. Perey, in *Direct Interactions and Nuclear Reaction Mechanisms,* edited by E. Clementel and C. Villi (Gordon and Breach, New York, 1963), p. 125.
[35]F. Perey and B. Buck, Nucl. Phys. 32, 353 (1962).
[36]W. J. Thompson, J. L. Adams, and D. Robson, Phys. Rev. 173, 975 (1968).
[37]S. A. A. Zaidi and S. Darmodjo, Phys. Rev. Lett. 19, 1446 (1967); H. L. Harney and H. A. Weidenmüller, Nucl. Phys. A139, 241 (1969).
[38]G. W. Bund, Ph.D. thesis, University of Washington, 1968; G. W. Bund and J. S. Blair, Nucl. Phys. A144, 384 (1970).
[39]D. G. Kovar, N. Stein, and C. K. Bockelman, Nucl. Phys. A231, 266 (1974).
[40]W. R. Hering, A. D. Achterath, and M. Dost, Phys. Lett. 26B, 568 (1968).
[41]W. Darcey, A. F. Jeans, and K. N. Jones, Phys. Lett. 25B, 599 (1967).
[42]P. Mukherjee, K. V. Chalapati Rao, and I. Mukherjee, Nucl. Phys. A129, 535 (1969).